AD-A171 616 A BREAKDOWN SURFACE MODEL FOR THERMAL BACKSCATTERING FROM THE EXHAUST PLU..(U) FALCOVITZ (JOSEPH) HAIFA (ISRAEL) J FALCOVITZ JUN 86 NPS-67-86-002CR 1/1

UNCLASSIFIED N62271-84-M-3345 F/G 20/4 NL

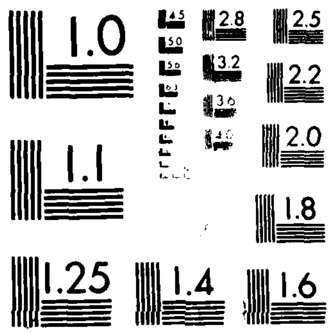

MICROCOPY RESOLUTION TEST CHART
NATIONAL BUREAU OF STANDA DS-1963-A

2

AD-A171 616

NPS67-86-002CR

NAVAL POSTGRADUATE SCHOOL

Monterey, California

CONTRACTOR REPORT

A BREAKDOWN SURFACE MODEL FOR THERMAL BACKSCATTERING FROM THE EXHAUST PLUME OF A SPACE-BASED HF LASER

Joseph Falcovitz

June 1986

Approved for public release; distribution unlimited.

Prepared for:

Strategic Defense Initiative Office
Washington, DC 20301-7100

NAVAL POSTGRADUATE SCHOOL
Monterey, California

RADM R. H. Shumaker
Superintendent

D. A. Schrady
Provost

The work reported herein was performed for the Naval Postgraduate School by Dr. Joseph Falcovitz under Contract N62271-84-M-3345. The work presented in this report is in support of "Rarefied Gas Dynamics of Laser Exhaust Plume" sponsored by the Strategic Defense Initiative Office/Directed Energy Office. This is the final report for that contract. The work provides information concerning backscattering to spacecraft from a multispecies laser exhaust plume. The project at the Naval Postgraduate School is under the cognizance of Distinguished Professor A. E. Fuhs who is principal investigator.

Prepared by:

Joseph Falcovitz

DR. JOSEPH FALCOVITZ
Research Contractor

Reviewed by:

Allen E. Fuhs

ALLEN E. FUHS
Distinguished Professor

M. F. Platzer

M. F. PLATZER
Chairman, Department of Aeronautics

Released by:

J. N. Dyer

J. N. DYER
Dean of Science and Engineering

UNCLASSIFIED
SECURITY CLASSIFICATION OF THIS PAGE

AD-A171 616

18 September 1985

REPORT DOCUMENTATION PAGE

1a REPORT SECURITY CLASSIFICATION UNCLASSIFIED	1b RESTRICTIVE MARKINGS NONE
2a SECURITY CLASSIFICATION AUTHORITY	3 DISTRIBUTION / AVAILABILITY OF REPORT Approved for Public Release; Distribution Unlimited
2b DECLASSIFICATION / DOWNGRADING SCHEDULE	
4 PERFORMING ORGANIZATION REPORT NUMBER(S) NPS67-86-002CR	5 MONITORING ORGANIZATION REPORT NUMBER(S) NPS67-86-002CR
6a NAME OF PERFORMING ORGANIZATION JOSEPH FALCOVITZ 6b OFFICE SYMBOL (If applicable) 67	7a NAME OF MONITORING ORGANIZATION NAVAL POSTGRADUATE SCHOOL, CODE 67
6c ADDRESS (City, State, and ZIP Code) Research Contractor Naval Postgraduate School, Code 67 Monterey, CA 93943-5100	7b ADDRESS (City, State, and ZIP Code) Department of Aeronautics Monterey, CA 93943-5100
8a NAME OF FUNDING / SPONSORING ORGANIZATION Strategic Defense Initiative Office 8b OFFICE SYMBOL (If applicable) SDIO/DEO	9 PROCUREMENT INSTRUMENT IDENTIFICATION NUMBER DGAM60045
8c ADDRESS (City, State, and ZIP Code) SDIO/DEO Washington, DC 20301-7100	10 SOURCE OF FUNDING NUMBERS PROGRAM ELEMENT NO: 9760400.2500 / PROJECT NO: 0801 / TASK NO: P6221 / WORK UNIT ACCESSION NO:

11 TITLE (Include Security Classification)
A BREAKDOWN SURFACE MODEL FOR THERMAL BACKSCATTERING FROM THE EXHAUST PLUME OF A SPACE-BASED HF LASER

12 PERSONAL AUTHOR(S)
JOSEPH FALCOVITZ

13a TYPE OF REPORT	13b TIME COVERED	14 DATE OF REPORT (Year, Month, Day)	15 PAGE COUNT
Contractor Report	FROM Sept. 85 TO Dec. 85	June 1986	

16 SUPPLEMENTARY NOTATION

17 COSATI CODES			18 SUBJECT TERMS (Continue on reverse if necessary and identify by block number)
FIELD	GROUP	SUB-GROUP	Laser Exhaust, Spacecraft Contamination, Chemical Laser, Exhaust Plume, Breakdown Surface

19 ABSTRACT (Continue on reverse if necessary and identify by block number)

The purpose of this report is to present a breakdown surface model for evaluating thermal backscattering flow from the supersonic exhaust plume of a gaseous mixture of H, HF, H_2, DF and He. Fluxes of these species are considered separately. The model is carefully analyzed and is shown to overestimate the flux. Actual flux levels of the heavy corrosive molecules (HD, DF) have been found to be exceedingly low. It is concluded that the contribution of thermal backscattering to contaminating flux of HF and DF can be neglected. This work is an extension and modification of the recent thesis work done by S. E. McCarty at the Naval Postgraduate School.

20 DISTRIBUTION / AVAILABILITY OF ABSTRACT ☒ UNCLASSIFIED/UNLIMITED ☐ SAME AS RPT ☐ DTIC USERS	21 ABSTRACT SECURITY CLASSIFICATION UNCLASSIFIED
22a NAME OF RESPONSIBLE INDIVIDUAL ALLEN E. FUHS, Distinguished Professor	22b TELEPHONE (Include Area Code): 408/646-2948 22c OFFICE SYMBOL: Code 72

DD FORM 1473, 84 MAR — 83 APR edition may be used until exhausted. All other editions are obsolete

SECURITY CLASSIFICATION OF THIS PAGE

☆ U.S. Government Printing Office: 1985—606-24.

ABSTRACT

The purpose of this report is to present a breakdown surface model for evaluating thermal backscattering flux from the supersonic exhaust plume of a space-based HF laser. The plume is of ring symmetry. It consists of a gaseous mixture of H, HF, H_2, DF and He. Fluxes of these species are considered separately. The model is carefully analyzed and is shown to overestimate the flux. Actual flux levels of the heavy corrosive molecules (HF, DF) have been found to be exceedingly low. It is concluded that the contribution of thermal backscattering to contaminating flux of HF and DF can be neglected. This work is an extension and modification of the recent thesis work done by S. E. McCarty at the Naval Postgraduate School.

ACKNOWLEDGEMENT

The ideas leading to this work crystalize through numerous discussions with LCDR Scott E. McCarty and Distinguished Professor Allen E. Fuhs. This Contractor report constitutes in fact an extension and generalization of LCDR McCarty's MSAE Thesis. Their help and cooperation are gratefully acknowledged.

TABLE OF CONTENTS

LIST OF FIGURES

1. INTRODUCTION

This report is a presentation of one part of a study on the contaminating backflow from the exhaust plume of a large space-based HF laser (Figure 1). The exhaust plume is an underexpanded supersonic ring-jet, designed to stay clear of the spacecraft by maintaining a Prandtl-Meyer turning angle at the nozzle lips of well below 90°. However, it is well known from experience with rocket plumes in space[1,2] that cavity regions (where continuum gasdynamic theory predicts vacuum) are filled with a free-molecular flow. This back flow is largely due to viscous effects, which give rise to a "spill-over" of the boundary layer around the nozzle lip[3]. Assuming the boundary layer can be eliminated (e.g., an expanding step design of the nozzle lip), there are two more mechanisms which lead to backflow: thermal backscattering and scattering by ambient molecules traveling at orbital speeds. Since these effects are a small perturbation to the exhaust flow field, they can be considered independently (the total backflow will be a superposition of contributions due to these two effects). As a first phase of our broader study, we consider solely the contribution of thermal backscattering to backflow from a ring-plume of an HF laser, via a simple model of molecular effusion from a breakdown surface, fashioned after ideas suggested by Noller[4]. Our results indicate that the backflow of the heavier contaminants (HF, DF) due to thermal backscattering is negligible.

Naturally, our study pertains to presumably typical operating conditions of the HF laser. These operating conditions were largely determined from a report on some HF laser tests conducted at TRW in 1971[5] (in particular, Table 5, Test III, of this report). The typical parameters at the nozzle exit

are:

Composition (mole fractions):	[H] = .091, [HF] = .091, [H_2] = .104, [DF] = .135, [He] = .579
Specific Heats Ratio:	γ = 1.54 (assuming ideal gas)
Mach Numbe	M_1 = 4.0
Average Molecular Weight	W_A = 7.27 [kg/kg mole] (1.1)
Stagnation Temperature	T_o = 2300 [K]
Stagnation Density	ρ_o = 0.0075 [kg/m^3]
Molecular Diameter, assuming it is uniform for all species (hard-sphere collisions)	D = 2.5 x 10^{-10} [m]

The exit Mach number can be chosen higher than M_1 = 4, but not considerably lower than this value, since M_1 = 4 results in a modest clearance angle of 41° between the limiting (vacuum) characteristic of the lip-centered rarefaction fan and the spacecraft. We assume isentropic flow throughout the diffuser[5], so that upon specifying the composition and flow variables at the diffuser inlet, along with M_1 at the diffuser exit, the exit flow is fully determined. One exception to this definition, however, is the stagnation temperature, which was estimated as T_o = 1400 [K] at the diffuser inlet[5]. We set T_o = 2300 [K], which corresponds to complete hydrogen recombination, even though the flow in the diffuser is of a nearly frozen composition due to the low rate of hydrogen recombination[5]. The reason for this choice is that given the uncertainty in determining T_o, which results from an uncertainty in the degree of hydrogen recombination, it is the most pessimistic choice, resulting in higher thermally backscattered flux.

The model that we propose for evaluating the backscattered flux arriving

at the spacecraft (Figures 1, 2) is based on the effusive breakdown surface concept suggested by Noller[4]. The gradual transition from continuum to collisionless flow, which invariably takes place at the outer fringes of exhaust plumes having a near-vacuum background environment, is replaced by an abrupt change. We assume that the flow regime in each stream tube changes from continuum (with local thermodynnamic equilibrium) to collisionless, upon crossing some breakdown surface.

An important simplification is introduced in the case of a large-radius spacecraft (about 2.5[m]), by observing that the temperature along the breakdown surface decreases so sharply with the distance from the nozzle lip, that the segment contributing significantly to thermal backscattering is only about 0.01 to 0.1[m] long. Consequently, the lip-centered rarefaction ring-fan may well be approximated by the standard (planar) Prandtl-Meyer flow field.

The structure of this report is as follows. The breakdown surface and the molecular effusion flux from it are obtained in closed-form expressions in Section 2. Section 3 is devoted to the spatial integration scheme, which is the evaluation of the flux arriving at a certain point on the spacecraft. Results of flux distribution along the spacecraft for the presumed laser operating range are presented and discussed in Section 4, followed by a critical examination of the breakdown surface model. Conclusions are given in Section 5, and Section 6 is a list of references. The code RINGBD, which computes the flux by numerical integration over the breakdown (effusing) surface, is given in Appendix A.

2. BREAKDOWN SURFACE AND EFFUSION FLUX

Our model for the thermally backscattered flux arriving at the surface of the spacecraft is essentially a modification of Noller's concept of a breakdown effusive surface[4]. We substitute his definition of a breakdown surface by a similar one introduced by Bird[6, Section 8.3]. We obtain the one-sided effusion flux from the breakdown surface by integrating over velocity space as suggested by Noller[4], except for the fact that we compute flux rather than density and we also consider the flux of species having molecular weight different from the average. In the following, each one of these steps is described in some detail, beginning with the breakdown surface.

As mentioned in the introduction, the lip-centered rarefaction fan is approximated by a planar Prandtl-Meyer flow field (Figure 2). The standard expressions for this flow field have Mach number (M) as the independent parameter, thus M varies between $M = M_1$ at the exit and $M \to \infty$ at the limiting (vacuum) characteristic. (Index 1 always refers to exit conditions, i.e., to parameters evaluated at $M = M_1$).

$$\psi(M) = -\zeta(M) + \zeta_1 + \mu_1 + \frac{\pi}{2}$$

$$\zeta(M) = \Gamma^{1/2} \, \mathrm{ARCTAN}\left[\Gamma^{-1/2}\left(M^2-1\right)^{1/2}\right] \qquad \Gamma = \left(\frac{\gamma+1}{\gamma-1}\right)$$

$$\mu(M) = \mathrm{ARCSIN}(M^{-1}) \tag{2.1}$$

$$\theta(M) = \psi(M) - \mu(M)$$

where ψ is the angle of characteristic lines, and θ is the angle of the velocity vector (or streamline).

Adopting Bird's definition of a breakdown parameter, which was first introduced in conjunction with a spherical source flow[6, Section 8.3] and later was shown to be meaningful also in a Prandtl-Meyer flow[7], we define the breakdown surface as having a constant value of B, where B is given by:

$$B = \frac{U}{\nu}\ \frac{1}{\rho}\left|\frac{d\rho}{dS}\right| \tag{2.2}$$

Here ρ, U, ν, S are local flow density, speed, collision frequency, and coordinate along streamlines (thus restricting this definition of B to stationary flows). From the geometrical relationships in a Prandtl-Meyer fan (Figure 2) and from (2.1) we get:

$$\frac{d\rho}{dS} = -\ (1/R)\ \left(\frac{d\rho}{d\psi}\right)\ \sin\mu = -\frac{2}{\gamma+1}\left[M^{-1}(M^2 - 1)^{1/2}\right]\ (\rho/R)$$

$$\rho(M) = \rho_o\ \left(1 + \frac{\gamma-1}{2}M^2\right)^{-\frac{1}{\gamma-1}} \tag{2.3}$$

Using the expression for collision frequency[6]:

$$\nu_o = 4(\pi/\gamma)^{1/2}\ \left(N_oD^2C_o\right) \tag{2.4}$$

where N_o,C_o,D are stagnation number density, stagnation sound speed, molecular diameter, and using U = MC in conjunction with (2.2) and (2.3), we get:

$$R_B(M) = (BN_oD^2)^{-1}\ \frac{(\gamma/\pi)^{1/2}}{2(\gamma+1)}\ \left(M^2-1\right)^{1/2}\ \left(1+\frac{\gamma-1}{2}M^2\right)^{\frac{1}{\gamma-1}} \tag{2.5}$$

This expression is almost identical to that of Bird[7], the main difference being in assuming a constant collision diameter (hard spheres), which we

believe to be commensurate with the overall crudeness of the model. The breakdown surface as defined by equations 2.5 and 2.1, starts at point $[R_B(M_1),\ \psi(M_1)]$ on the exit characteristic $M = M_1$, which we refer to as the intial point (see Figure 4). However, a breakdown in continuum flow also takes place on the segment of the exit characteristic between the corner and the intial point, since the value of the breakdown parameter there (Equation 2.2) is clearly larger than the value of B used in defining the breakdown surface (Equation 2.5). Hence, the breakdown surface defined by (2.5) should be supplemented by that segment. We refer to the combined surface as the augmented breakdown surface. The segment on the exit characteristic is referred to as the supplementary breakdown surface.

The one-sided directed effusion flux is defined as the number flux of molecules per unit area of an area element normal to the flux direction, per unit solid angle about the flux direction. It is obtained as a function of local Mach number and the angle κ between the flux direction and the local velocity vector, by repeating Noller's velocity integration scheme[4,EQ. (6)], with an added factor of molecular speed in order to obtain flux (rather than density as in Noller's work). The resulting expression for species i is readily obtained by using standard definite integrals:

$$
\begin{aligned}
F_i(M) = {} & h_i\, N_o C_o\, (W_A/W_i)^{1/2} \left(1 + \frac{\gamma-1}{2} M^2\right)^{-\frac{\gamma+1}{2(\gamma-1)}} \\
& \Big[(2\gamma\pi^3)^{-1/2} \left(1 + (1/2)\gamma\tilde{M}^2\cos^2\kappa\right) \mathrm{EXP}\left(-\gamma\tilde{M}^2/2\right) + \\
& (2\pi)^{-1}\, \tilde{M} \left(3/2 + (1/2)\gamma\tilde{M}^2\cos^2\kappa\right) \cos\kappa\ \mathrm{EXP}\left(-(1/2)\gamma\tilde{M}^2 \sin^2\kappa\right) \\
& \mathrm{ERFC}\left(-(\gamma/2)^{1/2}\, \tilde{M}\cos\kappa\right) \Big]
\end{aligned}
\qquad (2.6)
$$

$$\mathrm{ERFC}(v) = 2\,\pi^{-1/2} \int_v^\infty \mathrm{EXP}\,(-x^2)\,dx \qquad \text{(complementary error function)}$$

$\tilde{M} = (W_i/W_A)^{1/2}\ M$

h_i - Mole fraction of species i. (2.6 Continued)

W_i - Molecular weight of species i.

The dependence of $F_i(M)$ on the flux angle κ is so sensitive that for some Mach number around $M \approx 10$, the backflow (in the typical operating range) is virtually negligible. In the following section we describe how the flux $F_i(M)$ is integrated over the augmented breakdown surface, yielding the backscattered flux arriving at the surface of the spacecraft.

3. FLUX INTEGRATION

The effusion flux $F_i(M)$ given by (2.6) above, is defined in such a way that the number of molecules effusing from an area element ΔA_B of the breakdown surface and arriving at an area element ΔA_S on the spacecraft (per second), is given by:

$$F_i(M)\ (\Delta A_B \ \mathrm{COS}\ \alpha_B)\ (\Delta A_S\ \mathrm{COS}\alpha_S)\ L_{BS}^{-2}\ \text{[molecules per second]} \tag{3.1}$$

where α_B, α_S are the angles between the line-of-sight $\vec{L}_{BS}$ (Figure 3) and the normals to the breakdown surface and the spacecraft surface respectively. L_{BS} is the distance between the elements ΔA_B and ΔA_S. Dividing equation (3.1) by ΔA_S and integrating over the breakdown surface, the flux per unit area of the spacecraft is given by:

$$Q_i = \int F_i(M)\mathrm{COS}\alpha_B\ \mathrm{COS}\alpha_S\ L_{BS}^{-2}\ dA_B \quad \text{[Molecules per second per } m^2] \tag{3.2}$$

The integration scheme for Q_i over the breakdown surface is expressed in terms of the set of polar coordinates R, ψ, ϕ (Figure 3). For a point (R, ψ, ϕ) on the breakdown surface, using Cartesian coordinates (X, Y, Z) and the angle ω between X-axis and the line-of-sight $\vec{L}_{BS}$ we obtain the following geometrical relationships:

$$X = R\ \mathrm{COS}\psi \quad ; \quad Y = (A_o + R\ \mathrm{SIN}\psi)\ \mathrm{COS}\phi \quad ; \quad Z = (A_o + R\ \mathrm{SIN}\psi)\mathrm{SIN}\phi$$

$$\mathrm{COS}\phi_{MAX}(M) = \left(\frac{A_o}{A_o+R(M)\mathrm{SIN}\psi}\right) \tag{3.3}$$

$$\vec{U} = U(\mathrm{COS}\theta,\ \mathrm{SIN}\theta\ \mathrm{COS}\phi,\ \mathrm{SIN}\theta\ \mathrm{SIN}\phi)$$

$$\vec{L}_{BS}/|\vec{L}_{BS}| = (\mathrm{COS}\omega,\ \mathrm{SIN}\omega\ \mathrm{COS}\beta,\ \mathrm{SIN}\omega\ \mathrm{SIN}\beta)$$

$$\mathrm{TAN}\beta = \frac{Z}{(Y-A_o)}$$

The cosines $COS\kappa$, $COS\alpha_B$, $COS\alpha_S$ in (3.2) are expressed as scalar products of $[\vec{L}_{BS}/|\vec{L}_{BS}|]$ and unit vectors along the local velocity vector $\vec{U}$, along the local normal to the breakdown surface and along the local normal to the spacecraft surface, correspondingly.

The integration is performed numerically in two phases, the first being the integration along the supplimentary breakdown surface (Figure 4). For this first phase, the straight line segment which constitutes the supplementary breakdown surface is divided into several intervals of length ΔR (typically 10 intervals). Each interval generates a half-strip by rotating it from $\phi = 0$ through $\phi = \phi_{max}(M_1)$. This strip is in turn subdivided into several sub-intervals of $\Delta\phi$ each (typically 10 intervals). The total flux arriving at X_s is obtained by summing contributions from each sub-interval (two-dimensional integration). When the integration along the supplementary breakdown surface is concluded, it is continued into the breakdown surface, where ΔR intervals are replaced by breakdown surface intervals that correspond to a fixed Mach number increment ΔM (typically $\Delta M=0.1$). The integration proceeds along the breakdown surface (2.5) until the contribution of the last ΔM strip is negligibly small. The computation time is modest (about 1 second CPU per X_s point, on IBM 3033 mainframe computer). The computations were carried out by a code RINGBD written specifically for this purpose. Further details of the scheme and programming can be obtained by reading this code which is given in Appendix A.

4. RESULTS AND DISCUSSION

4.1 Presentation of Results

The molecular flux backscattered to the spacecraft from the surface of continuum flow breakdown in the lip-centered rarefaction fan, has been computed for all five species H, HF, H_2, DF, He. The results are depicted in Figures 5 to 9 respectively. For each species two more cases were computed in addition to the nominal case (1.1), where the stagnation density ρ_o was replaced by $\rho_o/10$ and by ρ_o*10 (see Figures 5 to 9). This has been done in order to demonstrate the effect of variations in exit flow conditions on the flux. The particular choice of ρ_o was motivated by the fact that the effects of changing ρ_o are not obvious. The effects of changing the exit Mach number M_1 or the stagnation temperature T_o are rather obvious (a higher flux would result from either a decrease in M_1 or an increase in T_o). It turns out that for points lying not too near the nozzle lip ($X_s > 0.1$ m), the lower density flow generates a higher backscattered flux!

In addition to varying ρ_o, we also varied the breakdown parameter B, obtaining a surprising result. The computation was performed for a particular species (HF), and the results obtained upon replacing B=0.05 (nominal value) by B/2 and by B*2 are brought in Figure 10.

It turns out that the B/2 case has the higher flux. This is somewhat surprising, since a lower value of B in a centered rarefaction fan (equation 2.5) means that the breakdown of continuum flow takes place in a region further out from the corner. In a source flow (e.g., a spherical source), that implies lower density and temperature, which would give rise to lower thermally backscattered flux.

An explanation to these seemingly counterintuitive results, along with some deeper insight into the breakdown surface model as it is applied to a centered rarefaction flow, can be obtained by taking a close look at the flow field and the breakdown surface in the vicinity of the corner. We take up this matter in the following sections.

We conclude the presentation of results, by comparing the flux (in the nominal case) of the five species with each other (Figure 11). This figure underlines the fact that the flux of light species (H, H_2, He) is many orders of magnitude (typically 10^{15}) times that of heavy species (HF, DF). Indeed, these results demonstrate a well known effect: When an expanding gaseous mixture of light and heavy molecules experiences a breakdown of continuum flow, a separation of species takes place (see e.g., the work of Cattolica et. al. [8]).

4.2 The Breakdown Surface and Streamlines

Consider the parametric description $R_B(M)$ for the breakdown surface (Equation 2.5). Normalizing R relative to the exit mean free path λ_1, we get:

$$R_B(M) = R_B(M_1)\left[(M^2 - 1)/(M_1^2 - 1)\right]^{1/2} \left[\left(1 + \frac{\gamma-1}{2} M^2\right)/\left(1 + \frac{\gamma-1}{2} M_1^2\right)\right]^{\frac{1}{\gamma-1}}$$

$$R_B(M_1)/\lambda_1 = \left[(\gamma\pi/2)^{1/2}/(\gamma+1)B\right] (M_1^2 - 1)^{1/2} \qquad (4.1)$$

$$\lambda_1 = \left(2^{1/2}\pi D^2 N_o\right)^{-1} \left[1 + \frac{\gamma-1}{2} M_1^2\right]^{\frac{1}{\gamma-1}}$$

The normalized surface $R_B(M)/\lambda_1$ is thus independent of stagnation density, depending only on γ, M_1, B.

Let us now derive a parametric equation $R_s(M)$ for a streamline that enters the fan at point $R_s(M_1)$ on the exit characteristic. The following geometrical relationship is readily obtained by considering two characteristic lines ψ and $\psi+\Delta\psi$ and a streamline inclined at the Mach angle μ to them:

$$\frac{dR_s(\psi)}{d\psi} = - R_s(\psi)\ (\tan\mu)^{-1} \tag{4.2}$$

Using the standard Prandtl-Meyer functions (2.1), we get the following differential equation for $R_s(M)$:

$$\frac{1}{R_s(M)}\ \frac{dR_s(M)}{dM} = \left(\frac{\gamma+1}{2}\right) M\left(1 + \frac{\gamma-1}{2} M^2\right)^{-1} \tag{4.3}$$

This equation is readily integrated, giving:

$$R_S(M) = R_S(M_1)\ \left[\left(1 + \frac{\gamma-1}{2} M^2\right)/\left(1 + \frac{\gamma-1}{2} M_1{}^2\right)\right]^{\frac{\gamma+1}{2(\gamma-1)}} \tag{4.4}$$

As pointed out by Bird[7], there is a particular streamline $R_{sa}(M)$ which asymptotically approaches the breakdown surface for large M, since the ratio $R_s(M)/R_B(M)$ tends to a constant (not zero) when $M \to \infty$. (Strictly speaking, this holds only for hard-sphere molecules, i.e., only when $\omega = 0.5$ in[7]). The limit is:

$$\lim_{M\to\infty} \frac{R_s(M)}{R_B(M)} = \frac{R_s(M_1)}{R_B(M_1)} \left[\frac{M_1^2 - 1}{M_1^2 + \frac{2}{\gamma-1}}\right]^{1/2} \tag{4.5}$$

For the limiting streamline $R_{sa}(M)$, the ratio $R_{sa}(M)/R_B(M)$ should tend to 1. This determines the point $R_{sa}(M_1)$ at which the limiting streamline enters the fan, as well as the entire line $R_{sa}(M)$:

$$R_{sa}(M_1) = R_B(M_1)\ \left[\frac{M_1^2 + \frac{2}{\gamma-1}}{M_1^2 - 1}\right]^{1/2} \tag{4.6}$$

Clearly, $R_{sa}(M)$ is larger than $R_B(M)$ for any $M > M_1$, so that no streamline beyond $R_{sa}(M)$ can cross the breakdown surface. This pattern is shown in Figure 4, where $R_{sa}(M)$ is denoted "streamline 2", and "streamline 1" is the streamline $R_s(M_1) = R_B(M_1)$.

All this leads to the following observation regarding the continuum breakdown of the flow in a centered rarefaction fan[7]. Referring to Figure 4, the fluid entering the fan through the supplementary breakdown surface (i.e., through the exit characteristic between the corner and the initial point of streamline 1), experiences breakdown immediately upon crossing this surface. Every streamline between streamline 1 and streamline 2 crosses the breakdown surface at some Mach number $M > M_1$, and at that point the continuum flow breaks down. All fluid entering the fan beyond stream-line 2 will never pass through the breakdown surface, and hence will maintain a continuum flow regime all the way to infinity. Of course, that is only true for planar centered rarefaction fans. When the exhaust flow emerges from a nozzle of finite width, and especially when the exhaust jet has a ring symmetry (as in our case), the breakdown surface gradually curves in a balloonlike shape towards the opposite nozzle lip, forming the familiar plume pattern (Figure 1).

4.3 Analysis and Discussion of Results

The foregoing analysis is now used to explain the variation in back-scattered flux due to a change in exhaust flow conditions at the nozzle exit. Specifically, we consider a tenfold decrease in stagnation density (i.e., the case $\rho_0/10$), and hence a tenfold increase in the exit mean free path λ_1.

The effusion flux from the breakdown surface is proportional to the local density, so one would expect to observe a decrease in flux, rather than

an increase (see Figures 5 to 9, for $X_s > 0.1$ m). Other factors causing increased flux, must then be larger than 10 so that they more than offset the 1/10 factor in density. It turns out that these effects are mainly geometrical, in that a tenfold increase in λ_1 causes the domain of integration on the breakdown surface to increase more than tenfold. In the (X,Y) plane there is a tenfold "blowup" of the breakdown surface, due to the self-similar structure of the Prandtl-Meyer flow field. As a result of this "blowup" in (X,Y), the angular integration range ϕ_{max} also increases, albeit not linearly (Equation 3.3). Another geometrical effect is an increase in the flux incidence cosine factor $\cos\alpha_s$ (see Equation 3.2), which for points X_s sufficiently far from the nozzle lip, increases roughly tenfold (while the other cosine factor $\cos^{\alpha}{}_B$ is almost constant). All this provides a qualitative explanation for the observed increase in flux at far points ($X_s >$ 0.1 m).

As for the near range ($X_s < 0.1$ m), another effect becomes increasingly significant as X_s approaches the nozzle lip. The turning angle κ, by which backscattered molecules have to be deflected relative to the flow velocity vector in order to reach point X_s on the spacecraft (Figure 2), increases with the size of the breakdown surface (fixed M and X_s). Since the local effusion flux (Equation 2.6) decreases rather sharply as κ is increased, the net result is a tendency to get a reduced backscattered flux at near points such as $X_s = 0.01$ m (Figures 5 to 9).

We now turn to the effect of changing the value of the breakdown parameter B. From equation 4.1 it is clear that multiplying B by some factor

will have the same "blowup" effect as dividing λ_1 by the same factor. A tenfold decrease in B is thus geometrically equivalent to a tenfold decrease in ρ_o. However, since the local effusion flux at the breakdown surface is proportional to ρ_o while it is independent of B, the B/10 case will have ten times as much backscattered flux as the $\rho_o/10$ case. In order to illustrate the sensitivity of the flux estimates to an uncertainty in the appropriate value of B, we computed the cases B/2 and B*2 for one species (HF), and they are presented in Figure 10. The variation in flux relative to the nominal case (B = 0.05), is by a factor no larger than about 5. Results for other species were found to exhibit comparable variations.

Does this observation about the dependence of the breakdown surface on B agree with the breakdown surface appropriate to the far field of the exhaust plume? In stationary source flow into vacuum, and when $M \gg 1$, the breakdown parameter varies with radius as $B \sim R^{\delta-1}$ ($\delta = 1$ for cylindrical source, $\delta = 2$ for spherical source). In a ringjet, the stream tubes of the exhaust plume generally diverge at a rate higher than that of stream tubes in a cylindrical source flow, so the effective value of δ in a ringjet is $\delta > 1$. Hence, in this case the far field breakdown surface moves downstream along each stream tube as the value of B increases. This is indeed geometrically compatible with the fact that near the corner of the lip-centered rarefaction fan $B \sim R^{-1}$, as shown schematically in Figure 12. The dependence of the breakdown surface on B near the corner and in the far field, thus assures that complete breakdown surfaces corresponding to different values of B, do not intersect (Figure 12).

In the foregoing discussion it was pointed out that variations in flux caused by changes in parameters such as ρ_o and B, were directly related

to the self-similar structure of the Prandtl-Meyer flow field. It has been further shown that these variations are well-understood within the framework of the breakdown surface model and that they are not excessively large. Are we to conclude that the thermally backscattered flux estimates of the present model are also physically plausible and reliable? In the following section we take up this matter, arriving at some interesting conclusions about this model and its range of validity.

4.4 Critical Examination of the Model

Consider the centered rarefaction flow field of a compressible fluid negotiating an expansive corner at supersonic speed (Prandtl-Meyer flow). The streamlines of this flow field have an orderly "layered" structure, with each streamline curving around the corner, starting at its point of entrance into the fan (see Figure 4).

The present model is based on the stipulation that there is a point of continuum flow breakdown on each streamline, provided this streamline is not beyond a certain limiting streamline. Consider a sample molecule effusing from this breakdown point toward the spacecraft. It advances at constant speed along a straight line trajectory, traversing all inner streamlines. Since the flow velocity vector points away from the spacecraft, and since the flow is highly supersonic so that the velocity of most individual molecules does not differ much from the flow velocity (i.e., it is a "cold" flow), any collision of the sample molecule with a mainflow molecule will most probably divert the sample molecule away from the spacecraft. What is the probability that a sample molecule would traverse this cross flow collisionlessly? This probability is simply $\exp(-n)$, where n is the expected number of collisions along the straight-line trajectory from the point of breakdown to the spacecraft. In the typical operating conditions assumed here, we estimated n to be roughly about 10. Since this no-collision probability factor is ignored in the formulation of the present model, the backscattered flux may be exaggerated by a factor of $\exp(10)$ or about 10^4. We conclude that in all likelihood, the prediction of the breakdown surface model for thermally backscattered flux from a centered rarefaction flow, is substantially overestimated.

Can anything be done to improve the present model? One may be inclined to suggest at this point that the obvious remedy is to incorporate the no-collision probability factor into the model. Rather, we prefer to retain the breakdown surface model in its present form as a simple means of obtaining an overestimate to the thermally backscattered flux from a centered rarefaction flow. An improved model can be constructed by considering thermal backscattering from the entire flow field (tempered by the probability of no-collision), without resorting to the physically untenable notion of an abrupt transition from continuum flow to free molecular flow.

5. CONCLUSIONS

Some surprising similarity laws of the breakdown surface model were observed. It has been shown that they were a direct result of the self similar structure of the Prandtl-Meyer flow field to which the model was applied. Specifically, it was found (and shown plausible) that reduced values of either the exhaust stagnation density ρ_0, or the breakdown parameter B, caused higher backscattered flux.

The breakdown surface model for thermally backscattered flux from a centered rarefaction fan, has been shown to overestimate the flux arriving at the spacecraft. It is suggested that an improved model be constructed by considering thermal backscattering from the entire flow field, along with the probability factor for a side-scattered molecule traversing the main flow collisionlessly.

The molecular flux of corrosive species (HF, DF) arriving at the spacecraft (Figures 6 and 8) is no larger than about 10^7 (sec^{-1} m^{-2}), which is negligible since it corresponds to about 10^{-5} molecular monolayers per year. This conclusion is reliable since even this flux level is an overestimate.

The maximum thermally backscattered flux of light species (H, H_2, He) is in the range of 10^{20} to 10^{22} (sec^{-1} m^{-2}) (see Figures 5, 7, 9). Thus, we conclude that while thermal backscattering would contribute significantly to the flux of light molecules arriving at the spacecraft, it is utterly negligible as far as heavy molecules are concerned.

5. REFERENCES

(1) Chemical Propulsion Information Agency, "JANNAF Handbook, Rocket Exhaust Plume Technology, Chapter 6: Spacecraft Plume Contamination", CPIA Publication 263, June 1983.

(2) Chemical Propulsion Information Agency, "JANNAF 13th Plume Technology Meeting," Vol. I, Houston, TX, April 1982. CPIA Publication 357, April 1982.

(3) G. A. Bird, "Breakdown of Continuum Flow in Free Jets and Rocket Plumes", Proc. 12th Symp. on Rarefied Gas Dynamics. In Vol. 74, Progress in Aeronautics and Astronautics, Sam S. Fisher Editor, Published by AIAA 1981.

(4) H. B. Noller, "Approximate Calculation of Expansion of Gas From Nozzles into High Vacuum", The Journal of Vacuum Science and Technology, Vol. 3, 202-207, 1966.

(5) F. Mastrup, E. Broadwell, J. Miller and T. A. Jacobs, "Hydrogen Fluoride Laser Technology Study", Technical Report No. AFWL-TR-72-28, October 1972.

(6) G. A. Bird, Molecular Gas Dynamics, Clarendon Press, Oxford 1976.

(7) G. A. Bird, "Prandtl-Meyer Flow of a Finite Knudsen Number Gas", Proceedings of the Seventh Australian Conference on Hydrodynamics and Fluid Mechanics, 1980.

(8) R. J. Cattolica, R. J. Gallagher, J. B. Anderson and L. Talbot, "Aerodynamic Separation of Gases by Velocity Slip in Freejet Expansions", AIAA Journal, Vol. 17, P. 344, 1974. (Also Reprint AIAA-77-709).

APPENDIX A. The Computer Code RINGBD

We present a printout of the code RINGBD along with the reults of the nominal case (printout of actual run). This is preceded by a brief description of the subroutines and a summary of major variables with their code and report notations.

A.1 Description of Subroutines

MAIN PROGRAM	-	Computes flux integration by summation of segment contributions (centered). Printing of results.
INIDAT	-	Definition of all data (no input file). Preparatory evaluation of parameters. Printing of data.
FLUX	-	Evaluates flux emitted from a single point on breakdown surface (mean segment values) to a point on spacecraft (XS).
BREAKR	-	Computes point on breakdown surface for given Mach number.
BREAKM	-	Computes point on breakdown surface for mean Mach number of a segment.

A.2 Code Versus Report Notation

XC(I) - [AB] - Mole fraction of species AB. (I=1,2,3,4,5 corresponds to H, HF, H_2, DF, He).

WC(I) - W_i - Molecular weight of species i.

WAV - W_A - Average molecular weight

TO - T_o - Stagnation temperature

RHOO - ρ_o - Stagnation density

G - γ - Specific heat ratio

EM1 - M_1 - Exit Mach number

LAMDA1 - λ_1 - Exit mean free path

AO - A_o - Spacecraft radius

R - R - Distance from corner ($X=0$, $Y^2+Z^2 = A_o^2$).

DIST - L_{BS} - Distance between emitting point on breakdown surface and receiving point (XS) on spacecraft.

XS - X_s - Point on spacecraft ($X=X_s$, $Y=A_o$, $Z=0$).

PSI - ψ - Characteristic angle

AMU - μ - Mach angle

TETA - θ - Velocity vector angle

PHI - ϕ - Rotation angle for flux integration

W - ω - Angle between x-axis and line-of-sight $\vec{L}_{BS}$

BETA - β - Angle between Y-axis and projection of $\vec{L}_{BS}$ on (Y,Z) plane.

DMO - ΔM - Mach number increment for flux integration

EM - M - Mach number

PBIRD - B - Breakdown parameter

A.3 Code Listing (Run of Nominal Case):

```
$JOB           RINGBD,NOXREF                                              RIN00010
      IMPLICIT REAL*8(A-H,O-Z,$)                                          RIN00020
      COMMON /GAMA/G,G1,G2,G3,G4,G5,G6,G7,G8,G9,G10,G11,G12,G13,G14,G15,RIN00030
     1          G16,G17,G18,G19,G20                                       RIN00040
      COMMON /PAR/C0,EN0,EM1,D,TLIM,ETALIM,CLIM,EL0,Q0,T0,                RIN00050
     1         PBIRD,RBIRD,DM0,DEG,OMEGA,XSV(51)                          RIN00060
      COMMON /NPAR/NETA,NC,NT,NEM0,NPHI,NXS,NR0,NSPEC                     RIN00070
      COMMON /GEOM/APF,PAI,PAI2,SW,CW,BETA,SBETA,CBETA,PSI1,SPSI1,        RIN00080
     1          CPSI1,PSIF,SPSIF,CPSIF,AK,SK,CK,A0,RF,XF,YF,ZF,           RIN00090
     2          PHI,SPHI,CPHI,RMIN,RMAX,XS,DIST,                          RIN00100
     3          AMU1,ZETA1,XN,YN,ZN,PSIM,SPSIM,CPSIM,R0                   RIN00110
      COMMON /EPSIL/EPSQ,EPSETA,EPST,EPSC,EPSEM                           RIN00120
      COMMON /EXTREM/TEXT,ETAEXT,CEXT,REXT,PSIEXT,EMEXT,BEXT,QEXT         RIN00130
      COMMON /SPEC/WAV,XC(5),WC(5),WCR(5),XNAME(5),QC(5),FLUXC(5)         RIN00140
      DIMENSION DSUM(5)                                                   RIN00150
      PRINT 101                                                           RIN00160
  101 FORMAT('1'/1X,'RINGBD - FLUX INTEGRATION FROM BREAKDOWN',           RIN00170
     1        1X,'SURFACE'//)                                             RIN00180
C                                                                         RIN00190
      CALL INIDAT                                                         RIN00200
C                                                                         RIN00210
      PRINT 110,XNAME                                                     RIN00220
  110 FORMAT(///1X,'  NX',' NEM','    XS    ',' PHIMAX','    QMAX   ',    RIN00230
     1        5(4X,A6,1X,'/ LOG',1X))                                     RIN00240
      DO 200 NX=1,NXS                                                     RIN00250
      EM=EM1                                                              RIN00260
      CALL BREAKR(EM,RF)                                                  RIN00270
      IF(NR0.GT.0) RF=R0                                                  RIN00280
      XF=RF*CPSI1                                                         RIN00290
      YF=RF*SPSI1+A0                                                      RIN00300
      XS=XSV(NX)                                                          RIN00310
      QMAX=0.                                                             RIN00320
      DO 45 N=1,NSPEC                                                     RIN00330
      FLUXC(N)=0.                                                         RIN00340
   45 CONTINUE                                                            RIN00350
      DO 1 NEM=1,NEM0                                                     RIN00360
      RN=RF                                                               RIN00370
      XN=XF                                                               RIN00380
      YN=YF                                                               RIN00390
      IF(NEM.GT.NR0) GO TO 41                                             RIN00400
      RF=R0+DFLOAT(NEM)*(RMIN-R0)/DFLOAT(NR0)                             RIN00410
      XF=RF*CPSI1                                                         RIN00420
      YF=RF*SPSI1+A0                                                      RIN00430
      RMEAN=(RN+RF)/2.D0                                                  RIN00440
      EMMEAN=EM1                                                          RIN00450
      PSIM=PSI1                                                           RIN00460
      SPSIM=SPSI1                                                         RIN00470
      CPSIM=CPSI1                                                         RIN00480
      GO TO 42                                                            RIN00490
   41 CONTINUE                                                            RIN00500
      EM=EM+DM0                                                           RIN00510
      CALL BREAKR(EM,RF)                                                  RIN00520
      EMMEAN=EM-DM0/2.D0                                                  RIN00530
      CALL BREAKM(EMMEAN,RMEAN)                                           RIN00540
   42 CONTINUE                                                            RIN00550
      ALONG=DSQRT((XF-XN)**2+(YF-YN)**2)                                  RIN00560
      SALFA=(YF-YN)/ALONG                                                 RIN00570
      CALFA=(XF-XN)/ALONG                                                 RIN00580
      PHIMAX=DARCOS(A0/(A0+RMEAN*SPSIM))                                  RIN00590
      DPHI=PHIMAX/NPHI                                                    RIN00600
```

```
      DO 44 N=1,NSPEC                                                   RIN00610
      DSUM(N)=0.                                                        RIN00620
   44 CONTINUE                                                          RIN00630
      DO 2 NP=1,NPHI                                                    RIN00640
      PHI=(DFLOAT(NP)-0.5D0)*DPHI                                       RIN00650
      CALL FLUX(EMMEAN,RMEAN)                                           RIN00660
      CROSS1=SW*CBETA                                                   RIN00670
      CROSS2=(SALFA)*(-CW)+(-CALFA*CPHI)*(-SW*CBETA)+                   RIN00680
     1       (-CALFA*SPHI)*(-SW*SBETA)                                  RIN00690
      GOREM=CROSS1*CROSS2*DPHI*(A0+RMEAN*SPSIM)*ALONG/DIST**2           RIN00700
      DO 24 N=1,NSPEC                                                   RIN00710
      DSUM(N)=DSUM(N)+QC(N)*GOREM                                       RIN00720
   24 CONTINUE                                                          RIN00730
      IF(QMAX.GE.QEXT) GO TO 25                                         RIN00740
      QMAX=QEXT                                                         RIN00750
   25 CONTINUE                                                          RIN00760
C     PRINT 22,NEM,NP,EMMEAN,RMEAN,PHIMAX*DEG,DARCOS(CW)*DEG,           RIN00770
C    1         BETA*DEG,PHI*DEG,CROSS1,CROSS2,ALONG,DIST,GOREM,         RIN00780
C    2         SPSIM,A0,(QC(N),FLUXC(N),N=1,NSPEC)                      RIN00790
C22   FORMAT(/1X,'NEM,NP,EMMEAN,RMEAN,PHIMAX=',2I3,3D13.4/              RIN00800
C    1       1X,'W,BETA,PHI=',3D15.5/                                   RIN00810
C    2       1X,'CROSS1,CROSS2,ALONG,DIST,GOREM=',5D15.5/               RIN00820
C    3       1X,'SPSIM,A0=',2D15.5/                                     RIN00830
C    4       1X,'QC,FLUXC=',5(1X,D10.3,1X,D10.3))                       RIN00840
    2 CONTINUE                                                          RIN00850
      DO 26 N=1,NSPEC                                                   RIN00860
      FLUXC(N)=FLUXC(N)+DSUM(N)                                         RIN0087C
   26 CONTINUE                                                          RIN00880
      IF(NEM.LE.NR0+2) GO TO 1                                          RIN00890
      DO 27 N=1,NSPEC                                                   RIN00900
      IF((DSUM(N)/FLUXC(N)).GT.EPSEM) GO TO 28                          RIN00910
   27 CONTINUE                                                          RIN00920
      GO TO 10                                                          RIN00930
   28 CONTINUE                                                          RIN00940
    1 CONTINUE                                                          RIN00950
   10 CONTINUE                                                          RIN00960
      DO 31 N=1,NSPEC                                                   RIN00970
      FLUXC(N)=2.D0*XC(N)*FLUXC(N)                                      RIN00980
   31 CONTINUE                                                          RIN00990
      PRINT 11,NX,NEM,XS,PHIMAX*DEG,QMAX,                               RIN01000
     1         (FLUXC(N),DABS(DLOG10(FLUXC(N))),N=1,NSPEC)              RIN01010
   11 FORMAT(/1X,2I4,F9.4,F7.2,D11.3,5(1X,D10.3,'/',F5.2))              RIN01020
  200 CONTINUE                                                          RIN01030
      PRINT 102                                                         RIN01040
  102 FORMAT(///1X,'END RINGBD RUN',///)                                RIN01050
      STOP                                                              RIN01060
      END                                                               RIN01070

      SUBROUTINE INIDAT                                                 RIN01080
      IMPLICIT REAL*8(A-H,O-Z,$)                                        RIN01090
      REAL*8 LAMDA0,LAMDA1                                              RIN01100
      COMMON /GAMA/G,G1,G2,G3,G4,G5,G6,G7,G8,G9,G10,G11,G12,G13,G14,G15,RIN01110
     1           G16,G17,G18,G19,G20                                    RIN01120
      COMMON /PAR/C0,EN0,EM1,D,TLIM,ETALIM,CLIM,EL0,Q0,T0,              RIN01130
     1          PBIRD,RBIRD,DM0,DEG,OMEGA,XSV(51)                       RIN01140
      COMMON /NPAR/NETA,NC,NT,NEM0,NPHI,NXS,NR0,NSPEC                   RIN01150
      COMMON /GEOM/APF,PAI,PAI2,SW,CW,BETA,SBETA,CBETA,PSI1,SPSI1,      RIN01160
     1           CPSI1,PSIF,SPSIF,CPSIF,AK,SK,CK,A0,RF,XF,YF,ZF,        RIN01170
     2           PHI,SPHI,CPHI,RMIN,RMAX,XS,DIST,                       RIN01180
     3           AMU1,ZETA1,XN,YN,ZN,PSIM,SPSIM,CPSIM,R0                RIN01190
```

```
      COMMON /EPSIL/EPSQ,EPSETA,EPST,EPSC,EPSEM                         RIN01200
      COMMON /EXTREM/TEXT,ETAEXT,CEXT,REXT,PSIEXT,EMEXT,BEXT,QEXT       RIN01210
      COMMON /SPEC/WAV,XC(5),WC(5),WCR(5),XNAME(5),QC(5),FLUXC(5)       RIN01220
      DATA XC/.091D0,.091D0,.104D0,.135D0,.579D0/                       RIN01230
      DATA WC/1.00D0,20.0D0,2.00D0,21.0D0,4.00D0/                       RIN01240
      DATA XNAME/'   H  ','  HF  ','  H2  ','  DF  ','  HE  '/          RIN01250
      PAI=4.*DATAN(.1D 1)                                               RIN01260
      AR=8.3143D3                                                       RIN01270
      AV=6.022D 26                                                      RIN01280
C  OMEGA=0.5 IS FOR HARD SPHERE COLLISIONS,                             RIN01290
C  AN AVERAGE RECOMMENDED VALUE IS ABOUT OMEGA=0.75                     RIN01300
      OMEGA=0.5D0                                                       RIN01310
      NSPEC=5                                                           RIN01320
      WAV=0.                                                            RIN01330
      DO 51 N=1,NSPEC                                                   RIN01340
      WAV=WAV+XC(N)*WC(N)                                               RIN01350
   51 CONTINUE                                                          RIN01360
      DO 52 N=1,NSPEC                                                   RIN01370
      WCR(N)=DSQRT(WC(N)/WAV)                                           RIN01380
   52 CONTINUE                                                          RIN01390
      A0=2.5D0                                                          RIN01400
      EM1=4.0D0                                                         RIN01410
      RHO0=0.0075D0                                                     RIN01420
      T0=2.300D3                                                        RIN01430
      D=2.50D-10                                                        RIN01440
      G=1.54D0                                                          RIN01450
      EN0=RHO0*AV/WAV                                                   RIN01460
      C0=DSQRT(G*AR*T0/WAV)                                             RIN01470
      PBIRD=0.05D0*2.D0                                                 RIN01480
C  R0 IS THE RADIUS FOR BEGINNING THE INTEGRATION ALONG THE M=M1        RIN01490
C  CHARACTERISTIC(THE AUGMENTED BREAKDOWN SURFACE).                     RIN01500
C  NR0 IS THE NUMBER OF INTEGRATION INTERVALS ON THIS SEGMENT.          RIN01510
C  FOR NO INTEGRATION ALONG M=M1 CHARACTERISTIC, SET NR0=0.             RIN01520
      R0=0.                                                             RIN01530
      NR0=10                                                            RIN01540
      DM0=0.1D0                                                         RIN01550
      NEM0=20.D0/DM0+NR0                                                RIN01560
C  TO GET FLUX DUE TO AUGMENTED BREAKDOWN SURFACE SOLELY, ACTIVATE:     RIN01570
C     NEM0=NR0                                                          RIN01580
      NPHI=10                                                           RIN01590
      NXS=13                                                            RIN01600
      XSI=1.D-2                                                         RIN01610
      XSF=1.D1                                                          RIN01620
      XSV(1)=XSI                                                        RIN01630
      IF(NXS.EQ.1) GO TO 111                                            RIN01640
      DXL=(DLOG(XSF)-DLOG(XSI))/(NXS-1.D0)                              RIN01650
      XLI=DLOG(XSI)                                                     RIN01660
      DO 11 NX=2,NXS                                                    RIN01670
      XSV(NX)=DEXP(XLI+(NX-1.D0)*DXL)                                   RIN01680
   11 CONTINUE                                                          RIN01690
  111 CONTINUE                                                          RIN01700
      EPSEM=1.D-5                                                       RIN01710
      DEG=180.D0/PAI                                                    RIN01720
      PAI2=PAI/2.D0                                                     RIN01730
      GAMMA=G                                                           RIN01740
      G1=(G-1.D0)/2.D0                                                  RIN01750
      G2=(G+1.D0)/(2.D0*(G-1.D0))                                       RIN01760
      G3=G/2.D0                                                         RIN01770
      G4=(G+1.D0)/(G-1.D0)                                              RIN01780
      G5=DSQRT((G+1.D0)/(G-1.D0))                                       RIN01790
```

```
      G6=1.D0/(G-1.D0)                                                  RIN01800
      G7=2.D0/(G+1.D0)                                                  RIN01810
      G8=(5.D-1*(G+1.D0)**2/(G-1.D0))**(1.D0/(G+1.D0)) *                RIN01820
     1   ((G+1.D0)/(G-1.D0))**((G-1.D0)/(G+1.D0))                       RIN01830
      G9=(G+3.D0)/(2.D0*(G-1.D0))                                       RIN01840
      G10=(7.D0-3.D0*G)/(2.D0*(G-1.D0))                                 RIN01850
      G11=DSQRT(G/PAI)/(2.D0*(G+1.D0))                                  RIN01860
      G12=DSQRT(G/2.D0)                                                 RIN01870
      G13=1.D0/DSQRT(2.D0*G*PAI**3)                                     RIN01880
      LAMDA0=1.D0/(DSQRT(2.D0)*PAI*D**2*EN0)                            RIN01890
      LAMDA1=LAMDA0*(1.D0+G1*EM1**2)**(G6-OMEGA+0.5D0)                  RIN01900
      RBIRD=G11/(D**2*EN0*PBIRD)                                        RIN01910
      ZETA1=G5*DATAN(DSQRT(EM1**2-1.D0)/G5)                             RIN01920
      AMU1=DARSIN(1.D0/EM1)                                             RIN01930
      PSI1=PAI2+AMU1                                                    RIN01940
      SPSI1=DSIN(PSI1)                                                  RIN01950
      CPSI1=DCOS(PSI1)                                                  RIN01960
      PSIF=PAI2+AMU1+ZETA1-G5*PAI2                                      RIN01970
      SPSIF=DSIN(PSIF)                                                  RIN01980
      CPSIF=DCOS(PSIF)                                                  RIN01990
      CALL BREAKR(EM1,RMIN)                                             RIN02000
      RSMIN=RMIN*DSQRT((2.D0/(G-1.D0)+EM1**2)/(EM1**2-1.D0))            RIN02010
C                                                                       RIN02020
      PRINT 201,NSPEC,XNAME                                             RIN02030
  201 FORMAT(/1X,'SPECIES DATA   NSPEC=',I3/                            RIN02040
     1         1X,'SPECIES NAMES     ',11(2X,A6,2X))                    RIN02050
      PRINT 202,XC                                                      RIN02060
  202 FORMAT( 1X,'MOLE FRACTION XC=',11(F8.4,2X))                       RIN02070
      PRINT 203,WC                                                      RIN02080
  203 FORMAT( 1X,'MOL. WEIGHT   WC=',11(F8.4,2X))                       RIN02090
      PRINT 21,AR,AV,WAV,G,RHO0,T0,EN0,C0,D                             RIN02100
   21 FORMAT(/1X,'THERMODYNAMIC DATA'/                                  RIN02110
     1         1X,'AR,AV,WAV,GAMMA=',2X,2D14.5,2F9.3/                   RIN02120
     2         1X,'RHO0,T0,EN0,C0,D=',D12.4,F8.0,D13.5,2D12.4)          RIN02130
      PRINT 22,EM1,PSI1*DEG,PSIF*DEG,PBIRD,                             RIN02140
     1          A0,RMIN,RSMIN,R0,                                       RIN02150
     2          LAMDA0,LAMDA1,RMIN/LAMDA1,RSMIN/LAMDA1                  RIN02160
   22 FORMAT(/1X,'FLOW AND GEOMETRY DATA'/                              RIN02170
     1         1X,'EM1,PSI1,PSIF,PBIRD=',4F9.3/                         RIN02180
     2         1X,'A0,RMIN,RSMIN,R0=',F9.3,3D14.5/                      RIN02190
     3         1X,'LAMDA0,LAMDA1,RMIN/LAMDA1,RSMIN/LAMDA1=',4D13.4)     RIN02200
      PRINT 23,DM0,NPHI,NR0,EPSEM                                       RIN02210
   23 FORMAT(/1X,'INTEGRATION DATA'/                                    RIN02220
     1         1X,'DM0,NPHI,NR0,EPSEM=',F9.3,2I5,4X,D12.3)              RIN02230
      RETURN                                                            RIN02240
      END                                                               RIN02250

      SUBROUTINE FLUX(EM,R)                                             RIN02260
      IMPLICIT REAL*8(A-H,O-Z,$)                                        RIN02270
      COMMON /GAMA/G,G1,G2,G3,G4,G5,G6,G7,G8,G9,G10,G11,G12,G13,G14,G15,RIN02280
     1              G16,G17,G18,G19,G20                                 RIN02290
      COMMON /PAR/C0,EN0,EM1,D,TLIM,ETALIM,CLIM,EL0,Q0,T0,              RIN02300
     1             PBIRD,RBIRD,DM0,DEG,OMEGA,XSV(51)                    RIN02310
      COMMON /NPAR/NETA,NC,NT,NEM0,NPHI,NXS,NR0,NSPEC                   RIN02320
      COMMON /GEOM/APF,PAI,PAI2,SW,CW,BETA,SBETA,CBETA,PSI1,SPSI1,      RIN02330
     1              CPSI1,PSIF,SPSIF,CPSIF,AK,SK,CK,A0,RF,XF,YF,ZF,     RIN02340
     2              PHI,SPHI,CPHI,RMIN,RMAX,XS,DIST,                    RIN02350
     3              AMU1,ZETA1,XN,YN,ZN,PSIM,SPSIM,CPSIM,R0             RIN02360
      COMMON /EXTREM/TEXT,ETAEXT,CEXT,REXT,PSIEXT,EMEXT,BEXT,QEXT       RIN02370
      COMMON /SPEC/WAV,XC(5),WC(5),WCR(5),XNAME(5),QC(5),FLUXC(5)       RIN02380
```

```
      SPHI=DSIN(PHI)                                                    RIN02390
      CPHI=DCOS(PHI)                                                    RIN02400
      XMEAN=R*CPSIM                                                     RIN02410
      YMEAN=(A0+R*SPSIM)*CPHI                                           RIN02420
      ZMEAN=(A0+R*SPSIM)*SPHI                                           RIN02430
      TBETA=ZMEAN/(YMEAN-A0)                                            RIN02440
      BETA=PAI2-DATAN(1.D0/TBETA)                                       RIN02450
      SBETA=DSIN(BETA)                                                  RIN02460
      CBETA=DCOS(BETA)                                                  RIN02470
      DIST=DSQRT((XS-XMEAN)**2+(YMEAN-A0)**2+ZMEAN**2)                  RIN02480
      CW=-(XS-XMEAN)/DIST                                               RIN02490
      SW=DSQRT(1.D0-CW**2)                                              RIN02500
      GM=(1.D0+G1*EM**2)**(-G2)                                         RIN02510
      AMU=DARSIN(1.D0/EM)                                               RIN02520
      TETA=PSIM-AMU                                                     RIN02530
      STETA=DSIN(TETA)                                                  RIN02540
      CTETA=DCOS(TETA)                                                  RIN02550
      CKAPA=(CTETA)*(-CW)+(STETA*CPHI)*(-SW*CBETA)+                     RIN02560
     1      (STETA*SPHI)*(-SW*SBETA)                                    RIN02570
      SKAPA=DSQRT(1.D0-CKAPA**2)                                        RIN02580
      QEXT=0.                                                           RIN02590
      DO 1 N=1,NSPEC                                                    RIN02600
      EMT=EM*CKAPA*G12*WCR(N)                                           RIN02610
      IF(DABS(EMT).GT.13.D0) EMT=EMT*(13.D0/DABS(EMT))                  RIN02620
      POW=G3*EM**2*WCR(N)**2                                            RIN02630
      POWT=POW*SKAPA**2                                                 RIN02640
      IF(POW.GT.1.0D2)POW=1.0D2                                         RIN02650
      IF(POWT.GT.1.0D2) POWT=1.0D2                                      RIN02660
      EXP1=DEXP(-POW)                                                   RIN02670
      EXP2=DEXP(-POWT)                                                  RIN02680
      ERFC1=DERFC(-EMT)                                                 RIN02690
      IF(ERFC1.LT.1.D-43) ERFC1=1.D-43                                  RIN02700
C     IF(XS.LT.5.D0) GO TO 234                                          RIN02710
C     IF(EXP1.GT.1.D-20.AND.ERFC1.GT.1.D-20) GO TO  234                 RIN02720
C     PRINT 235,N,POW,POWT,EMT,EXP1,EXP2,ERFC1                          RIN02730
C235  FORMAT(I4,8D11.3)                                                 RIN02740
C234  CONTINUE                                                          RIN02750
      EVER1=EN0*(C0/WCR(N))*G13*GM*(1.D0+EMT**2)*EXP1                   RIN02760
      EVER2=(EN0*(C0/WCR(N))*0.5D0/PAI)*(EM*WCR(N))*CKAPA*GM*           RIN02770
     1       (1.5D0+EMT**2)*EXP2*ERFC1                                  RIN02780
      QC(N)=EVER1+EVER2                                                 RIN02790
      IF(QEXT.GE.QC(N)) GO TO 1                                         RIN02800
      QEXT=QC(N)                                                        RIN02810
    1 CONTINUE                                                          RIN02820
      RETURN                                                            RIN02830
      END                                                               RIN02840

      SUBROUTINE BREAKR(EM,R)                                           RIN02850
      IMPLICIT REAL*8(A-H,O-Z,$)                                        RIN02860
      COMMON /GEOM/APF,PAI,PAI2,SW,CW,BETA,SBETA,CBETA,PSI1,SPSI1,      RIN02870
     1             CPSI1,PSIF,SPSIF,CPSIF,AK,SK,CK,A0,RF,XF,YF,ZF,      RIN02880
     2             PHI,SPHI,CPHI,RMIN,RMAX,XS,DIST,                     RIN02890
     3             AMU1,ZETA1,XN,YN,ZN,PSIM,SPSIM,CPSIM,R0              RIN02900
      COMMON /PAR/C0,EN0,EM1,D,TLIM,ETALIM,CLIM,EL0,Q0,T0,              RIN02910
     1            PBIRD,RBIRD,DM0,DEG,OMEGA,XSV(51)                     RIN02920
      COMMON /GAMA/G,C1,G2,G3,G4,G5,G6,G7,G8,G9,G10,G11,G12,G13,G14,G15,RIN02930
     1             G16,G17,G18,G19,G20                                  RIN02940
      R=RBIRD*DSQRT(EM**2-1.D0)*(1.D0+G1*EM**2)**(G6-OMEGA+0.5D0)       RIN02950
      ZETA=G5*DATAN(DSQRT(EM**2-1.D0)/G5)                               RIN02960
      PSI=PAI2+AMU1+ZETA1-ZETA                                          RIN02970
```

```
      XF=R*DCOS(PSI)                                                    RIN02980
      YF=R*DSIN(PSI)+A0                                                 RIN02990
      ZF=0.                                                             RIN03000
    1 CONTINUE                                                          RIN03010
      RETURN                                                            RIN03020
C                                                                       RIN03030
      ENTRY BREAKM(EM,R)                                                RIN03040
C                                                                       RIN03050
      R=RBIRD*DSQRT(EM**2-1.D0)*(1.D0+G1*EM**2)**(G6-OMEGA+0.5D0)       RIN03060
      ZETA=G5*DATAN(DSQRT(EM**2-1.D0)/G5)                               RIN03070
      PSIM=PAI2+AMU1+ZETA1-ZETA                                         RIN03080
      SPSIM=DSIN(PSIM)                                                  RIN03090
      CPSIM=DCOS(PSIM)                                                  RIN03100
      RETURN                                                            RIN03110
      END                                                               RIN03120
$ENTRY                                                                  RIN03130
```

```
RINGBD - FLUX INTEGRATION FROM BREAKDOWN SURFACE

SPECIES DATA   NSPEC=  5
SPECIES NAMES          H          HF         H2         DF         HE
MOLE FRACTION XC=  0.0910     0.0910     0.1040     0.1350     0.5790
MOL. WEIGHT   WC=  1.0000    20.0000     2.0000    21.0000     4.0000

THERMODYNAMIC DATA
AR,AV,WAV,GAMMA=      0.83143D 04   0.60220D 27    7.270     1.540
RHOO,TO,ENO,CO,D=  0.7500D-02    2300.   0.62125D 24  0.2013D 04  0.2500D-09

FLOW AND GEOMETRY DATA
EM1,PSI1,PSIF,PBIRD=     4.000  104.478   41.044     0.100
A0,RMIN,RSMIN,RO=     2.500   0 30574D-02   0.34812D-02   0.00000D 00
LAMDA0,LAMDA1,RMIN/LAMDA1,RSMIN/LAMDA1=   0.5797D-05   0.1281D-03   0.2372D 02   0.2718D 02

INTEGRATION DATA
DMO,NPHI,NRO,EPSEM=    0.100   10   10        0.100D-04
```

NX	NEM	XS	PHIMAX	QMAX	H / LOG	HF / LOG	H2 / LOG	DF / LOG	HE / LOG
1	47	0.0100	11.19	0.120D 25	0.824D 22/21.92	0.269D 07/ 6.43	0.777D 21/20.89	0.691D 06/ 5.84	0.653D 20/19.81
2	50	0.0178	12.15	0.121D 25	0.474D 22/21.68	0.162D 07/ 6.21	0.424D 21/20.63	0.418D 06/ 5.62	0.349D 20/19.54
3	54	0.0316	13.50	0.122D 25	0.237D 22/21.38	0.776D 06/ 5.89	0.196D 21/20.29	0.202D 06/ 5.30	0.154D 20/19.19
4	59	0.0562	15.27	0.123D 25	0.106D 22/21.02	0.295D 06/ 5.47	0.780D 20/19.89	0.770D 05/ 4.89	0.568D 19/18.75
5	64	0.1000	17.16	0.124D 25	0.421D 21/20.62	0.892D 05/ 4.95	0.268D 20/19.43	0.233D 05/ 4.37	0.175D 19/18.24
6	70	0.1778	19.55	0.124D 25	0.149D 21/20.17	0.219D 05/ 4.34	0.791D 19/18.90	0.575D 04/ 3.76	0.451D 18/17.65
7	77	0.3162	22.52	0.124D 25	0.471D 20/19.67	0.464D 04/ 3.67	0.203D 19/18.31	0.122D 04/ 3.09	0.100D 18/17.00
8	84	0.5623	25.65	0.124D 25	0.132D 20/19.12	0.901D 03/ 2.95	0.461D 18/17.66	0.237D 03/ 2.37	0.201D 17/16.30
9	92	1.0000	29.39	0.124D 25	0.335D 19/18.52	0.167D 03/ 2.22	0.959D 17/16.98	0.440D 02/ 1.64	0.381D 16/15.58
10	100	1.7783	33.26	0.124D 25	0.771D 18/17.89	0.305D 02/ 1.48	0.187D 17/16.27	0.801D 01/ 0.90	0.699D 15/14.84
11	108	3.1623	37.22	0.124D 25	0.165D 18/17.22	0.548D 01/ 0.74	0.353D 16/15.55	0.144D 01/ 0.16	0.126D 15/14.10
12	116	5.6234	41.19	0.124D 25	0.332D 17/16.52	0.981D 00/ 0.01	0.648D 15/14.81	0.258D 00/ 0.59	0.227D 14/13.36
13	124	10.0000	45.14	0.124D 25	0.641D 16/15.81	0.175D 00/ 0.76	0.117D 15/14.07	0.461D-01/ 1.34	0.405D 13/12.61

```
END RINGBD RUN

STATEMENTS EXECUTED= 1281233
```

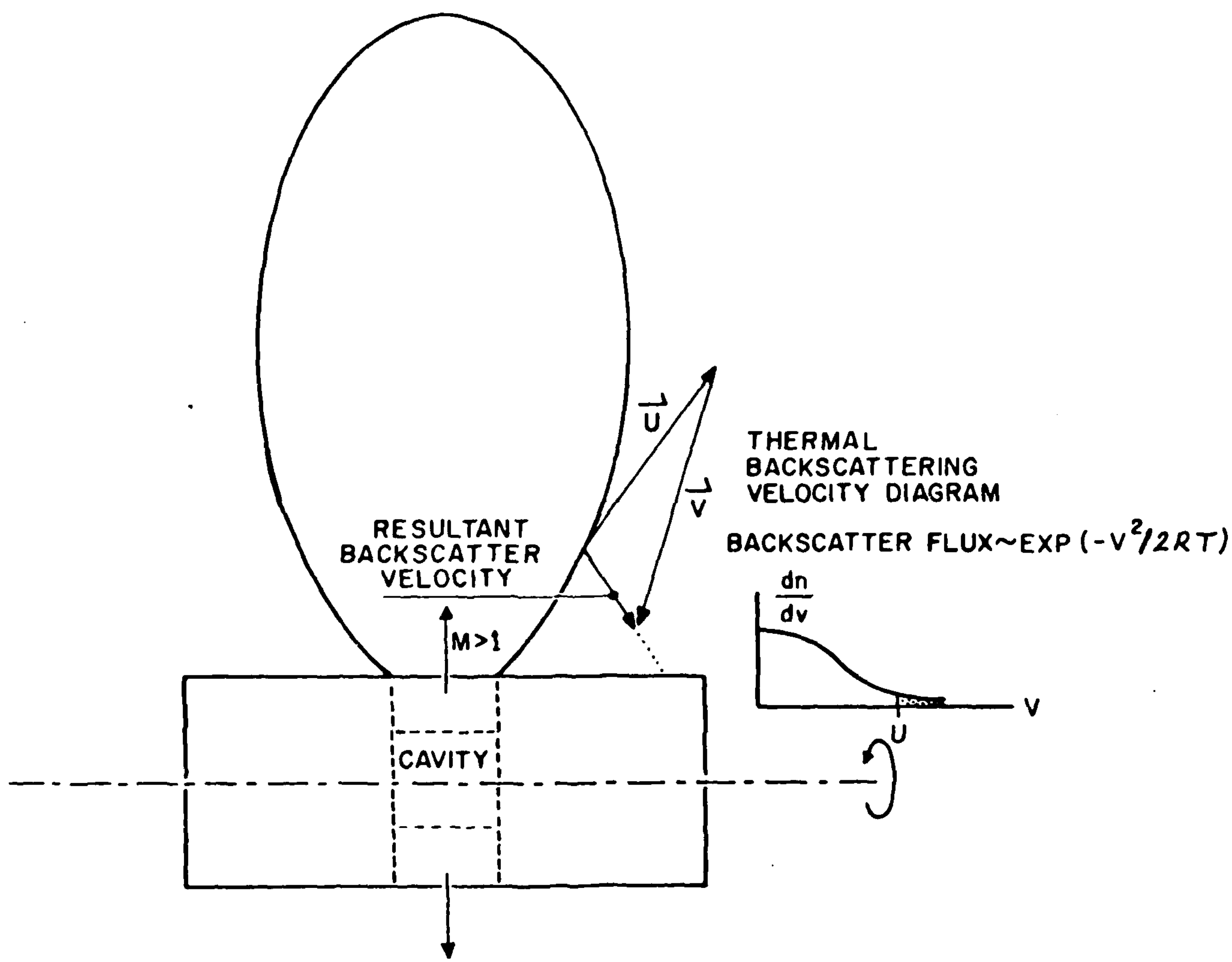

Figure 1. Thermal Backscattering from Laser Exhaust Plume

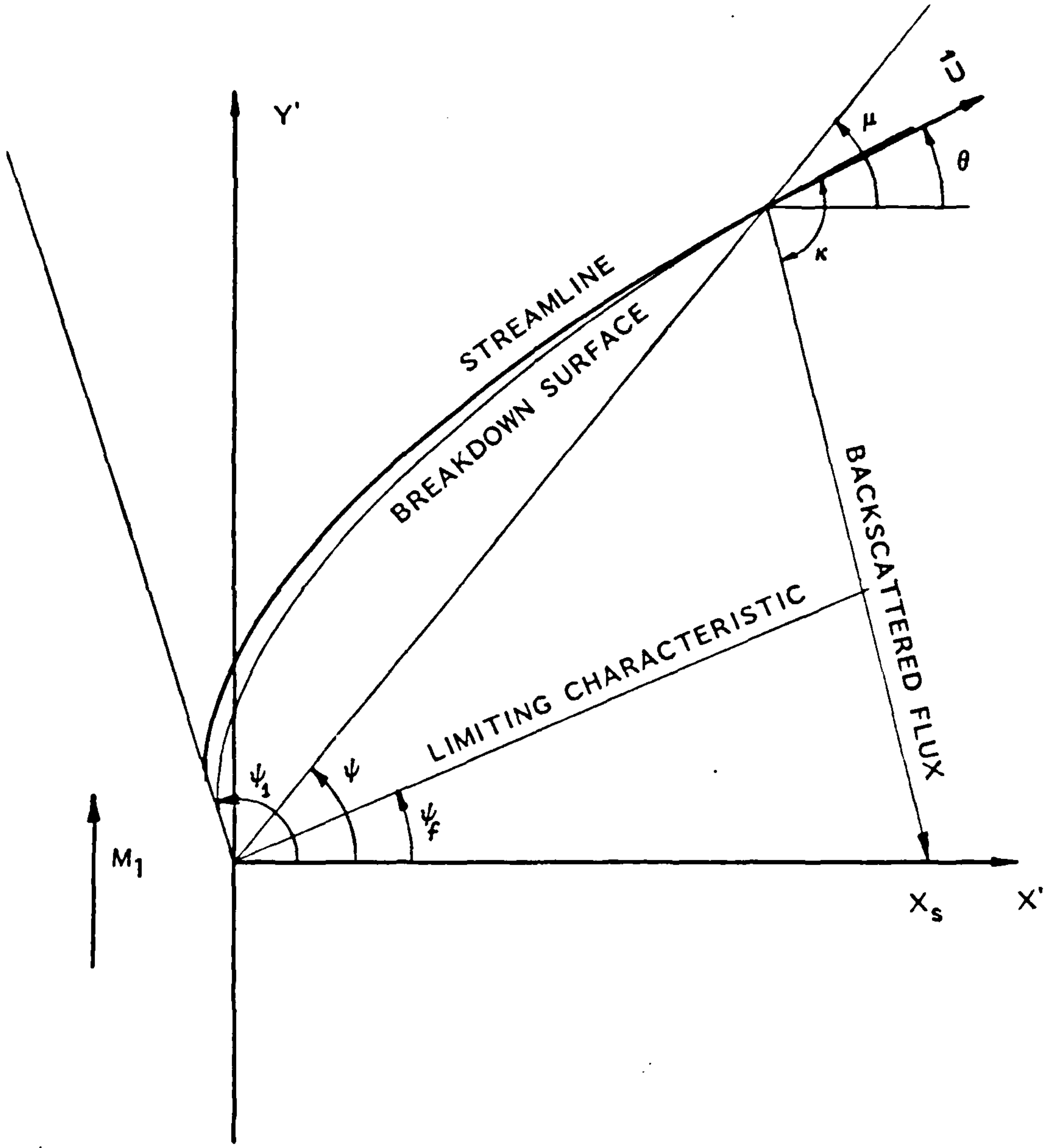

Figure 2. Prandtl-Meyer Centered Rarefaction Fan and Breakdown Surface (Schematic)

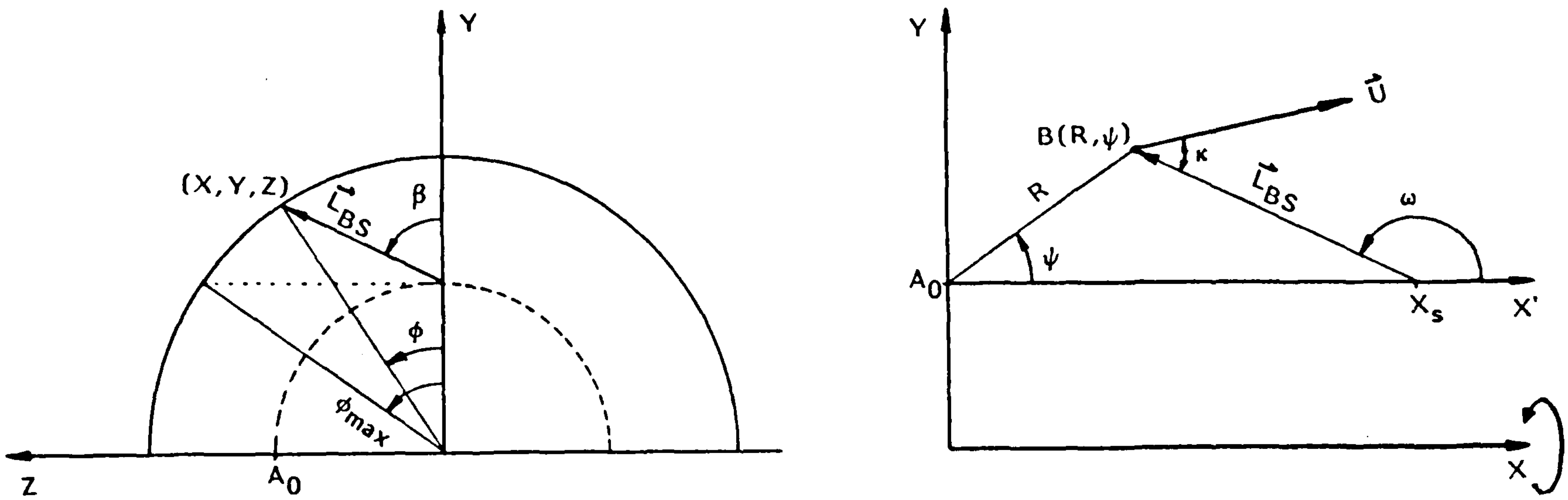

Figure 3. Flux Integration Scheme

B - Point on Breakdown Surface

(X,Y,Z) - Point on Breakdown Surface (Same point as B(R,ψ))

$\vec{L}_{BS}$ - Line of Sight

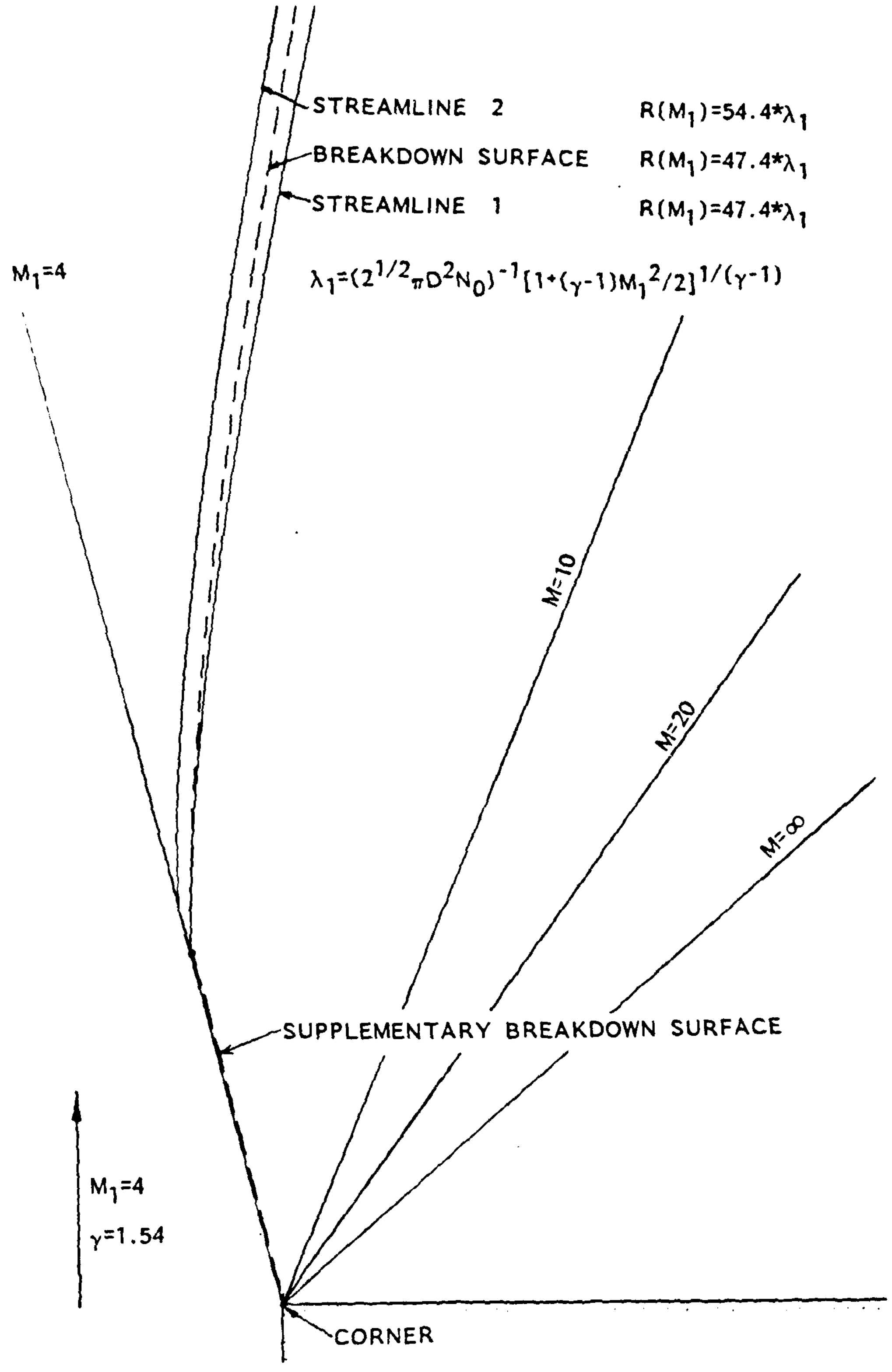

Figure 4. Prandtl-Meyer Flow Field Near the Corner, Including Actual Streamlines and Breakdown Surface

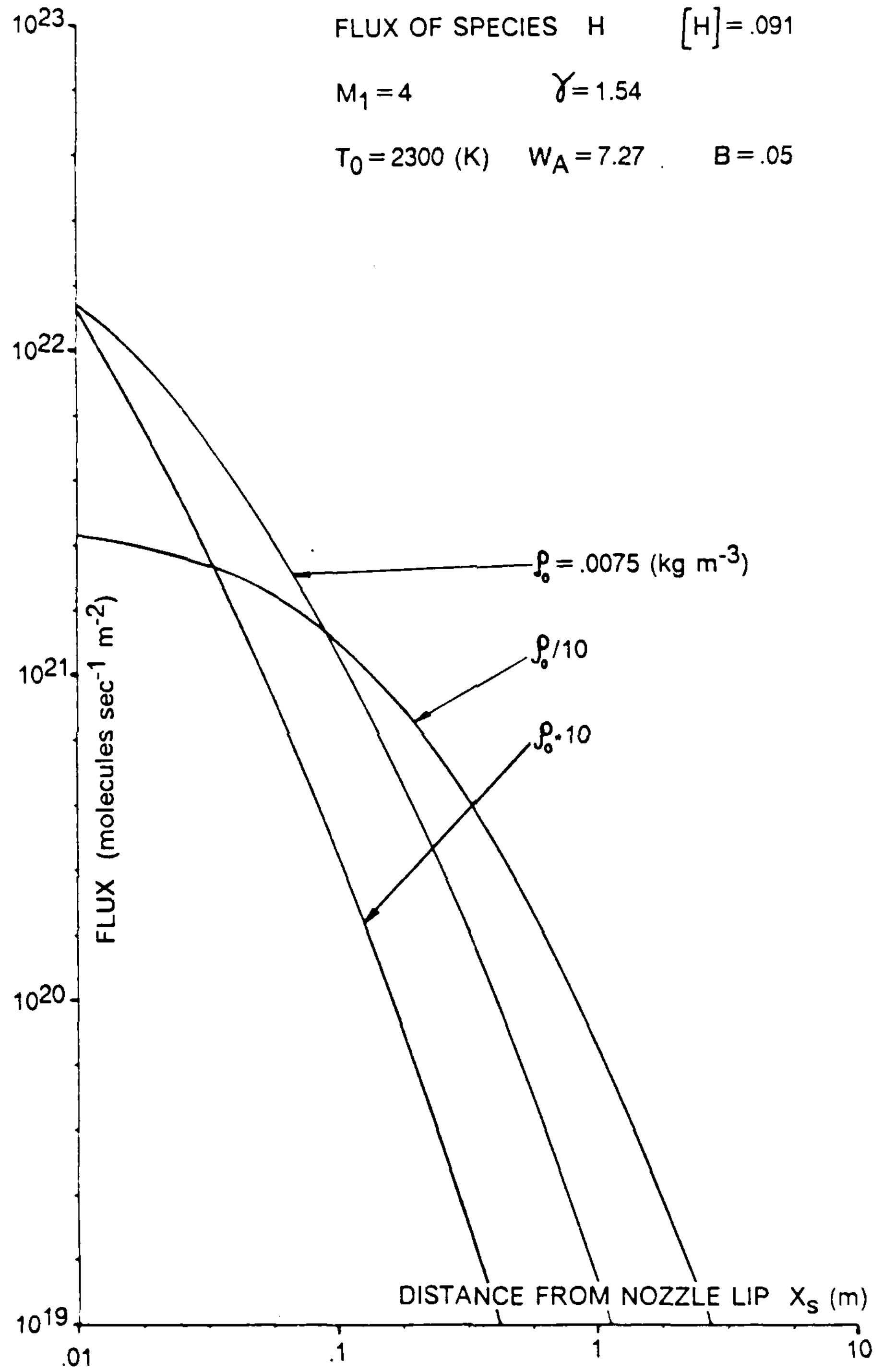

Figure 5. Flux of Species H at Various Stagnation Densities

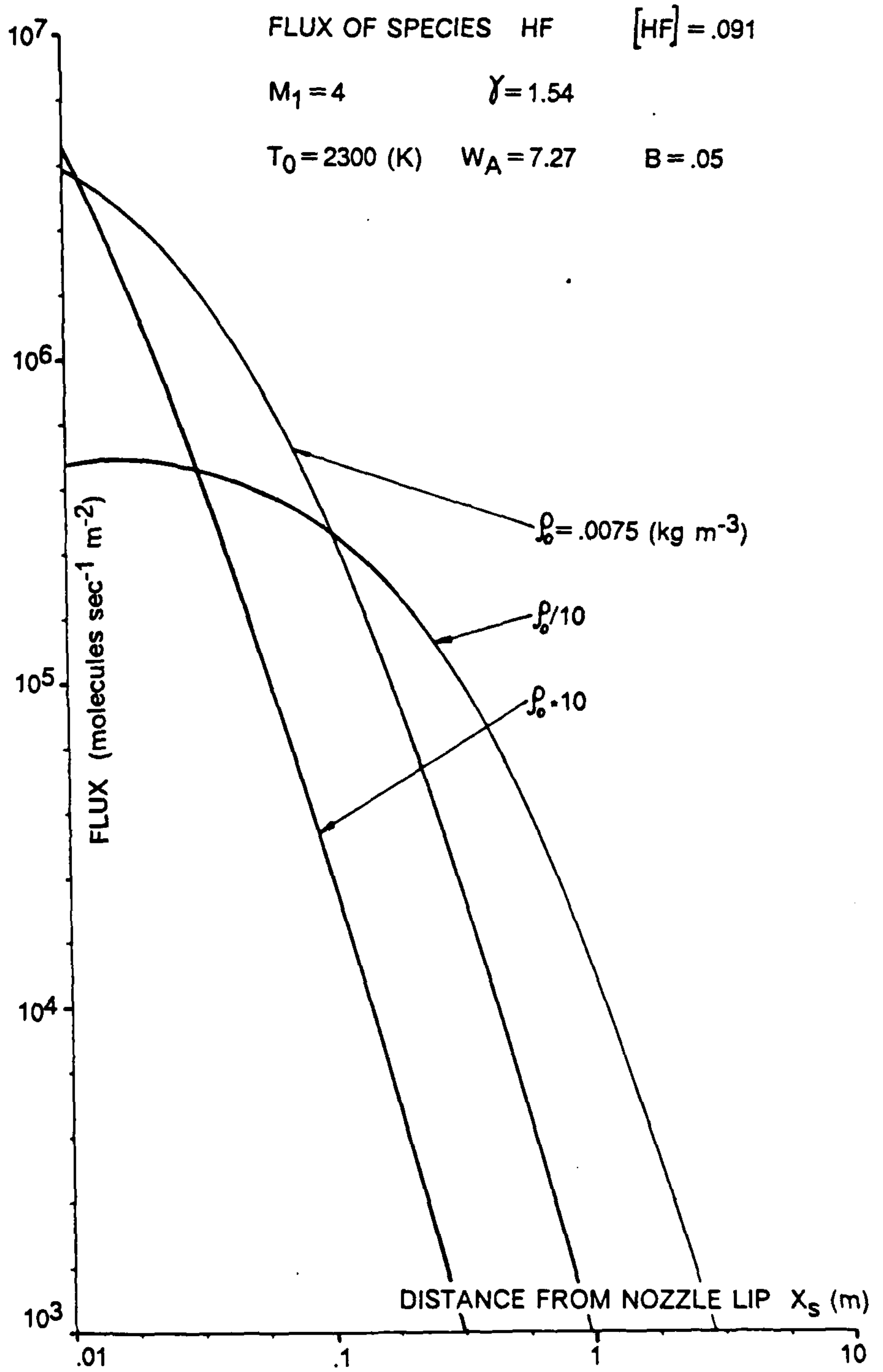

Figure 6. Flux of Species HF at Various Stagnation Densities

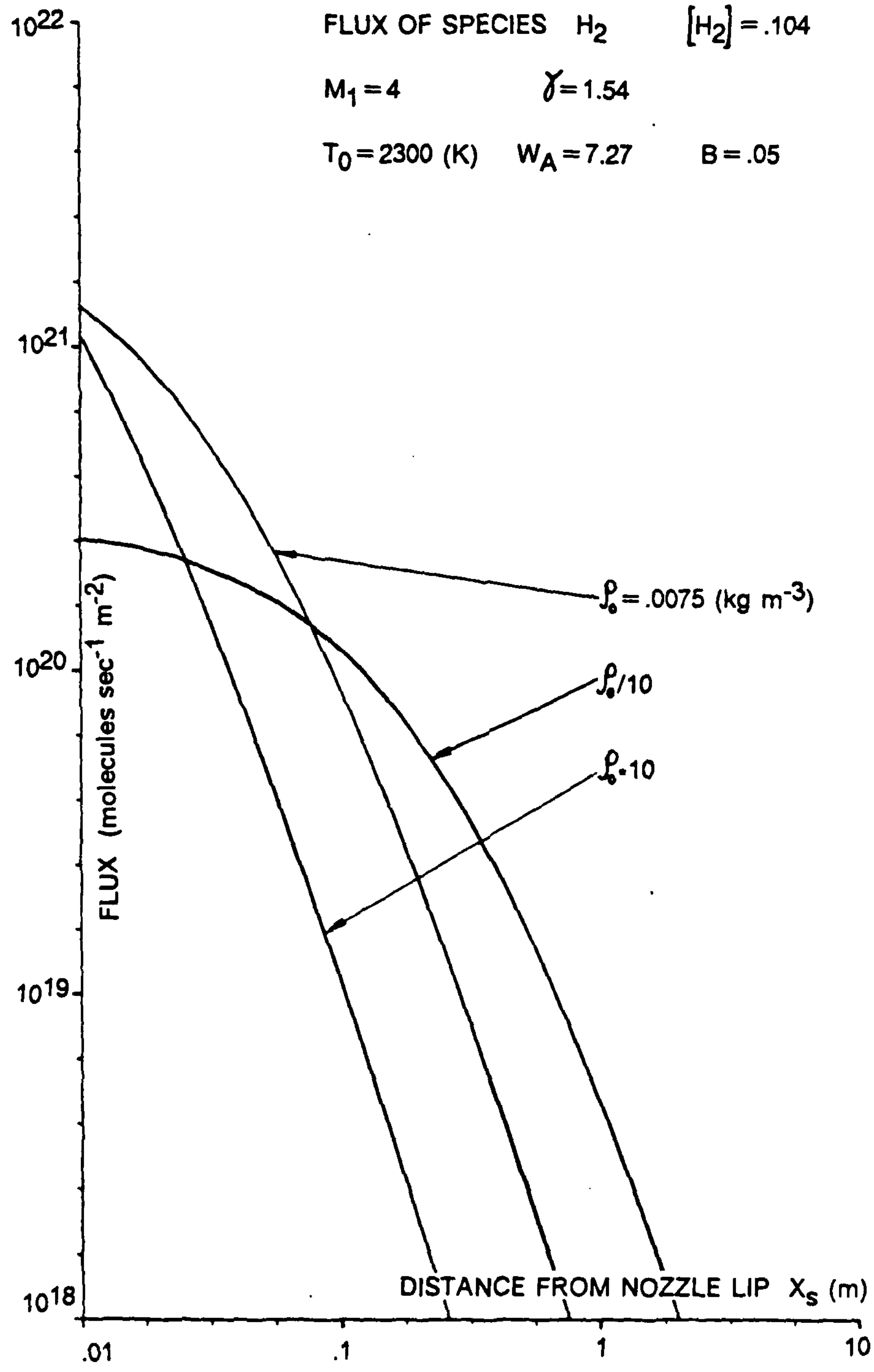

Figure 7. Flux of Species H_2 at Various Stagnation Densities

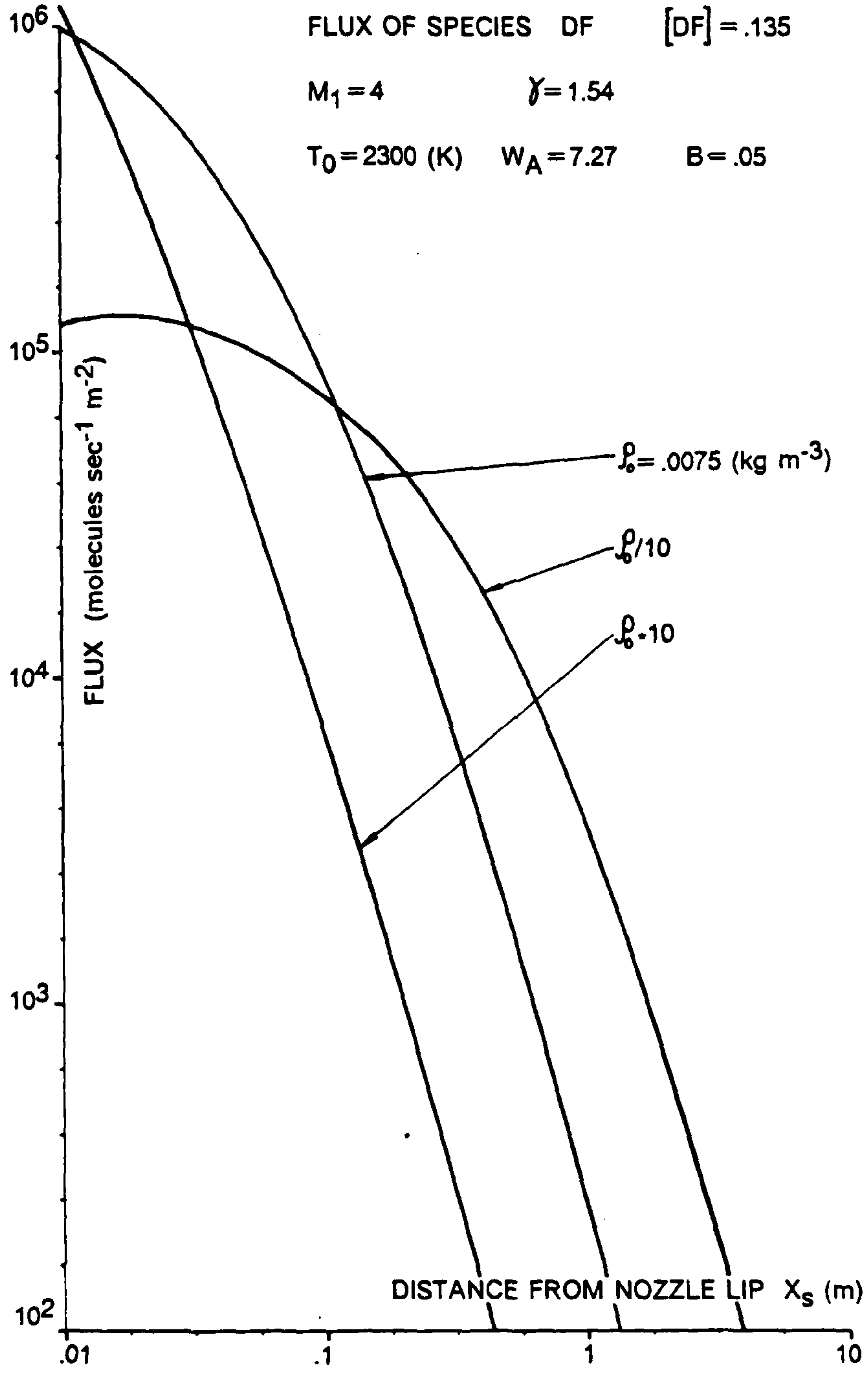

Figure 8. Flux of Species DF at Various Stagnation Densities

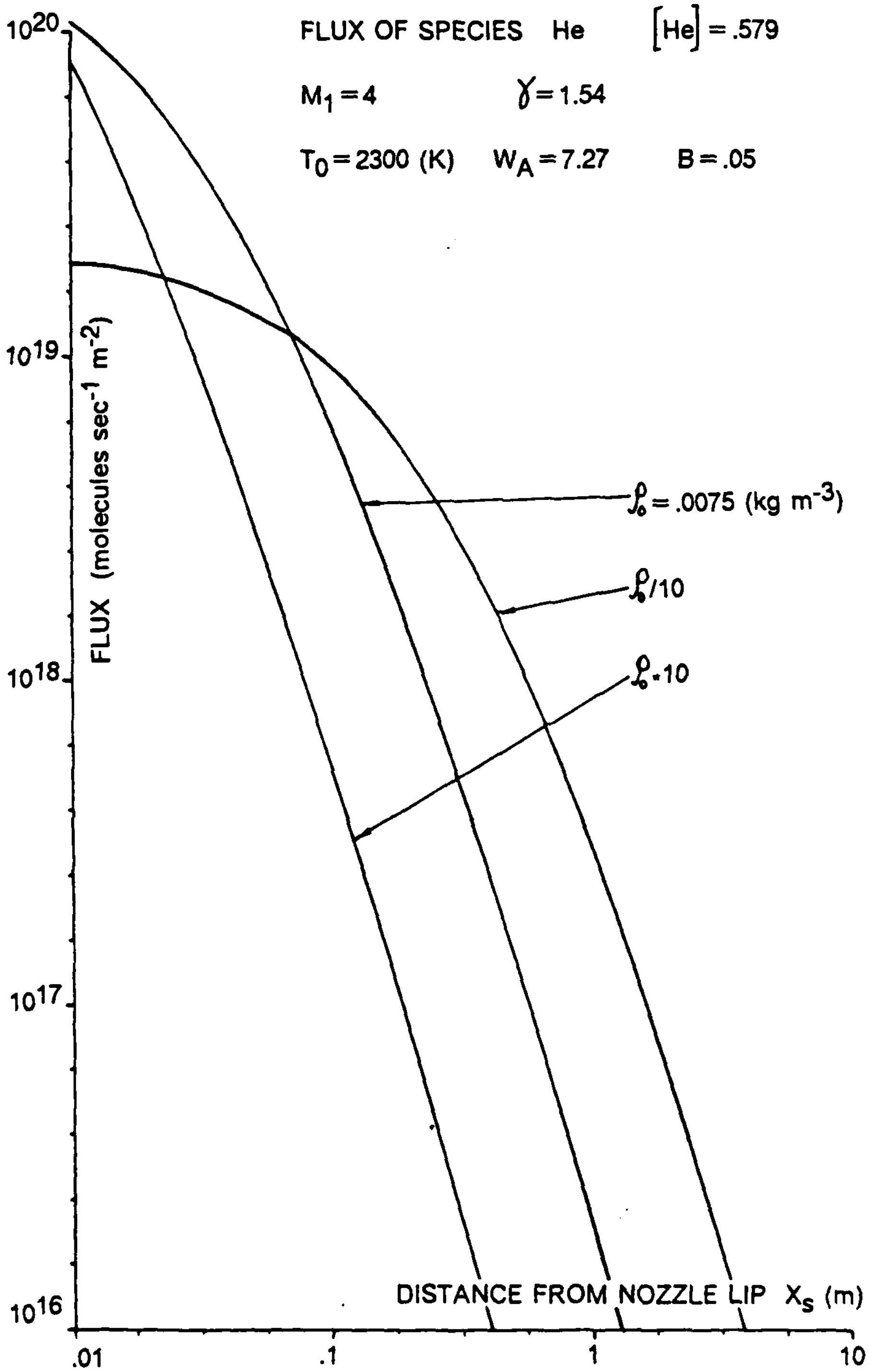

Figure 9. Flux of Species He at Various Stagnation Densities

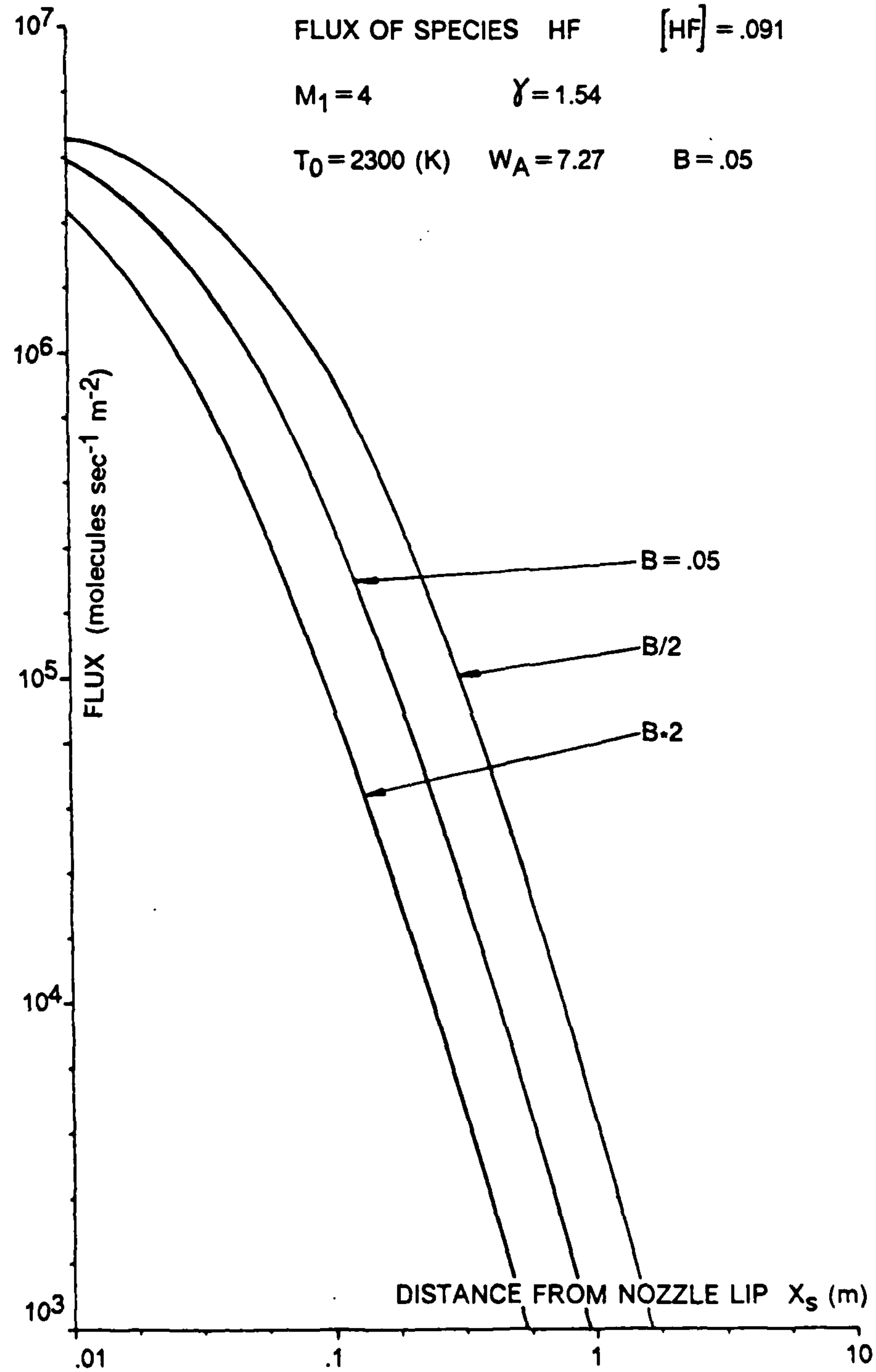

Figure 10. Flux of Species HF at Various Values of Breakdown Parameter

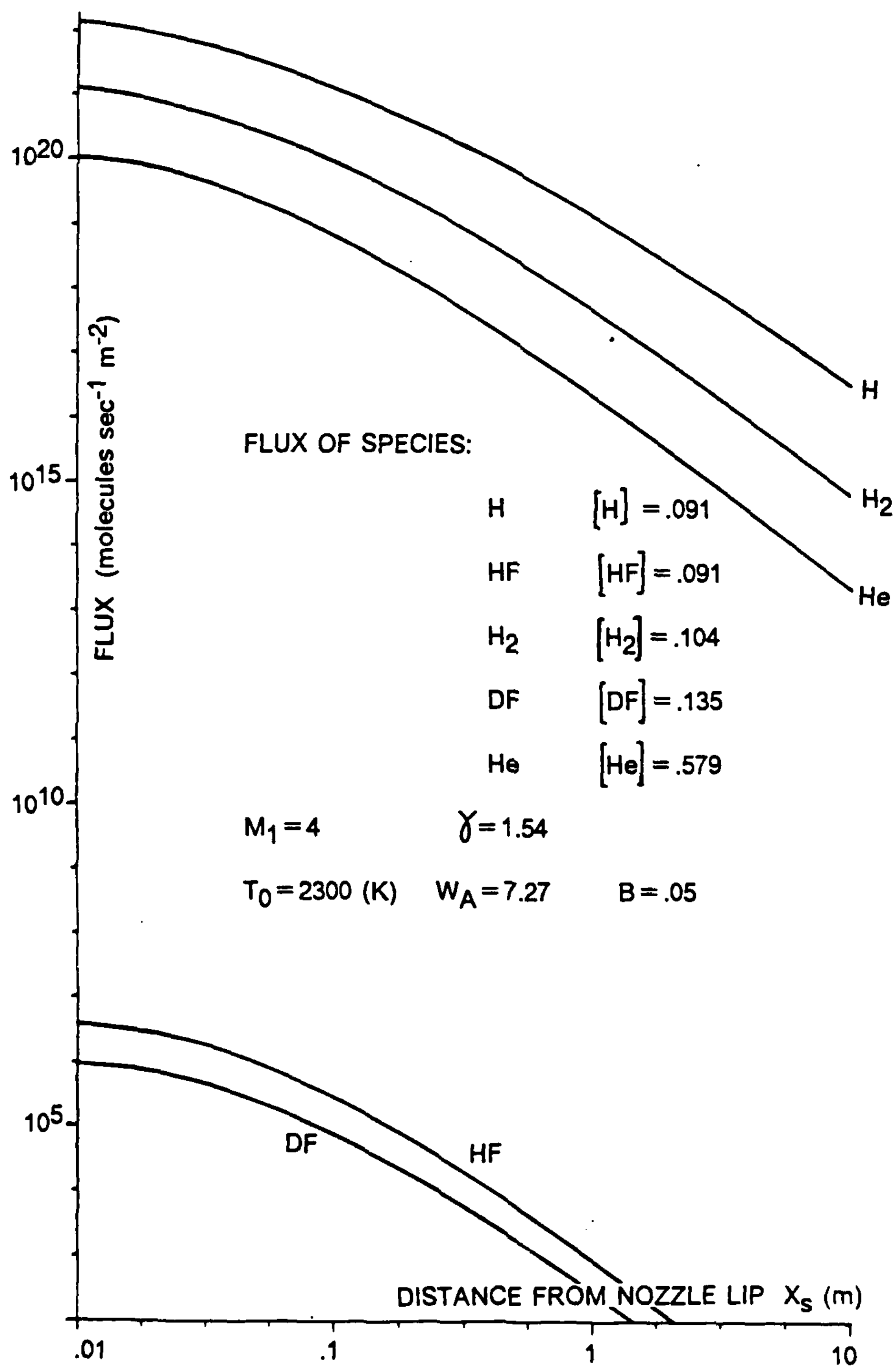

Figure 11. Flux of All Species at Typical Operating Conditions

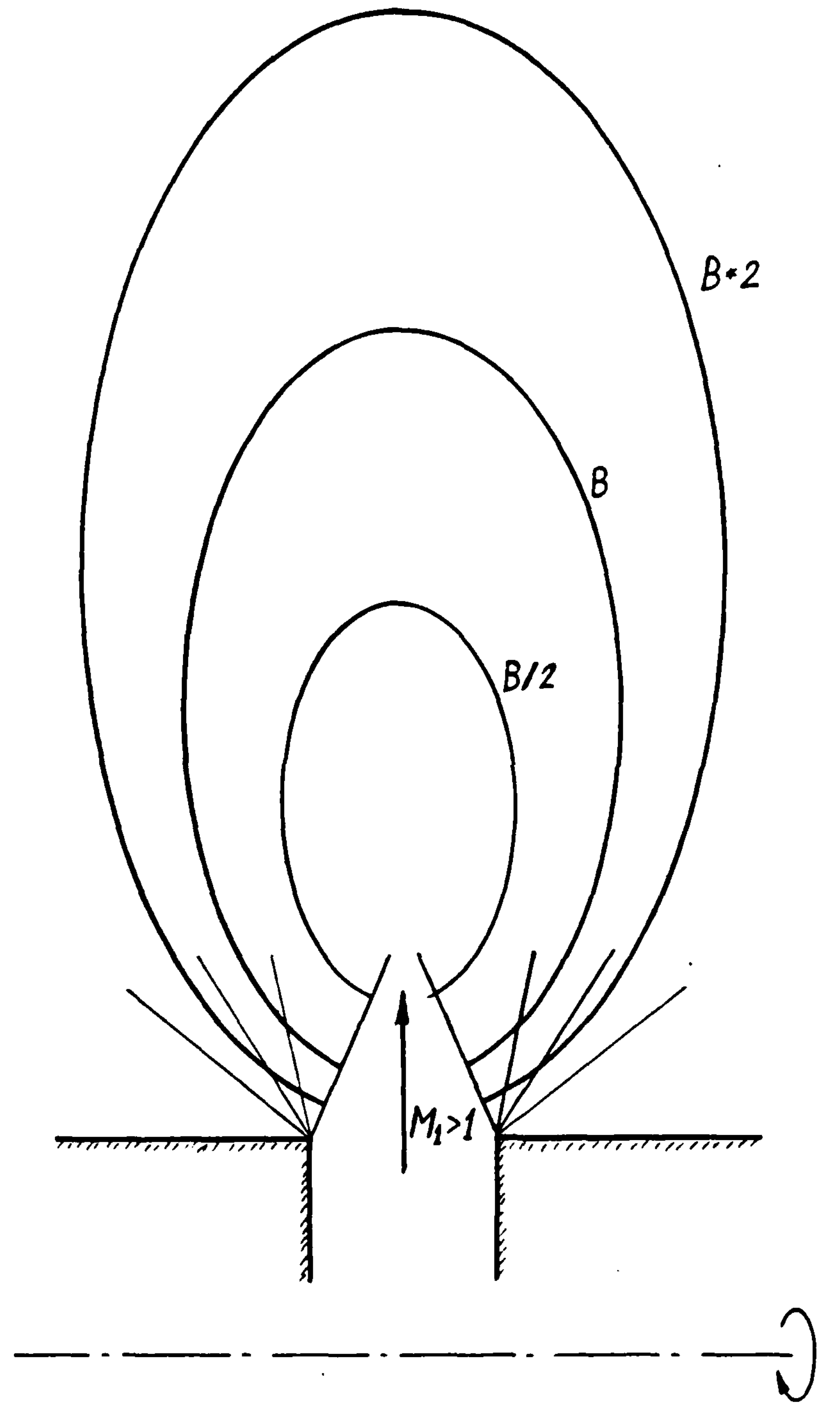

Figure 12. Schematic Display of Complete Breakdown Surface in a Ringjet Exhaust Plume

DISTRIBUTION LIST

		No. Copies
1.	Defense Technical Information Center Cameron Station Alexandria, Virginia 22314	2
2.	Library, Code 0142 Naval Postgraduate School Monterey, California 93943	2
3.	Department Chairman, Code 67 Department of Aeronautics Naval Postgraduate School Monterey, California 93943	1
4.	Distinguished Professor Allen E. Fuhs Code 72 Naval Postgraduate School Monterey, California 93943	4
5.	Mr. Neil Griff Pentagon SDIO/DEO Washington, DC 20301-7100	3
6.	Mr. Bruce Pierce Pentagon SDIO/DEO Washington, DC 20301-7100	1
7.	Dr. Joseph Falcovitz Code 72 Naval Postgraduate School Monterey, CA 93943-5100	8
8.	Associate Professor Oscar Biblarz Department of Aeronautics Code 67Bi Naval Postgraduate School Monterey, CA 93943-5100	1
9.	Dr. P. Avizonis Air Force Weapons Laboratory Kirtland Air Force Base, NM 87117	1
10.	Research Administration Office Code 012 Naval Postgraduate School Monterey, CA 93943-5100	1

END

10-86

DTIC